Homogenization of heterogeneous polymers towards Cosserat media

van der Sluis, O.

Award date:
1996

Homogenization of Heterogeneous Polymers towards Cosserat Media

O. van der Sluis

June 1996, WFW-report 96-090
Graduate thesis

Olaf van der Sluis

Eindhoven University of Technology
Department of Mechanical Engineering
Fundamentals of Mechanical Engineering (WFW)

Professor: Prof. Dr Ir H.E.H. Meijer

Coaches: Dr Ir P.H.J. Vosbeek
Dr Ir P.J.G. Schreurs
Ir R.J.M. Smit

Contents

Summary

During the mechanical loading of heterogeneous materials, such as composites, polymer blends and wood, micromechanical failure mechanisms like matrix crazing or cracking, void formation and fibre-matrix debonding occur. On the macroscopic level, these mechanisms may result in a decreasing stress with increasing strain. This is called strain softening. Experiments on polymer blends have shown that the influence of the microscopic configuration on the macroscopic behaviour is quite substantial. If the relation between the microscopic deformation and the macroscopic mechanical behaviour can be obtained, it will become possible to design new materials with desired properties such as high strength, high stiffness or high toughness.

The method for obtaining this relation is called homogenization. The heterogeneous (macroscopic) medium is replaced by a homogeneous continuum. The macroscopic state variables (stresses and strains) are defined in terms of those of the microscopic model and the evolution of the macroscopic state is established. This results in the determination of the constitutive relations.

Classical homogenization methods are based on the assumption that the material is statistically homogeneous. This means that all characteristic lengths are large compared to a distance within which the material properties undergo considerable variations about their mean value. In addition, the character of the variations within that distance in one part of the sample is of the same sort as the variations in another part of the sample. Only then, it is possible to associate a representative volume element (RVE) with each material point. Under these assumptions, the state of a material point can be defined as an appropriate average of the state of the RVE associated with that point. This will result in a macroscopic local constitutive equation that relates averages of the stress to averages of the strain. However, if a material exhibits strain softening behaviour and localization of deformation, the assumption of statistically homogeneity is no longer valid. In addition, the local models are incapable of describing localization phenomena. When long range effects are incorporated into the continuum mechanical description of the material, in the form of supplementary degrees of freedom, these non-local models are capable of describing strain softening. The obvious solution is to extend the state of the material point with additional statistical moments of the state of the RVE. Cosserat theory provides these additions in the form of rotational degrees of freedom. The relation between these degrees of freedom and the additional statistical moments have to be determined.

In this report, a polycarbonate plate with holes is used as a model material. The size of these holes is assumed to be small. Then, it is possible to identify an RVE, whose dimensions are small compared to the macroscopic length scales. To obtain a relation between the macroscopic deformation variables and the macroscopic consitutitive quantities, appropriate boundary conditions will be applied to the RVE. These boundary conditions are displacement fields, formulated in terms of the macroscopic deformation variables. From this, the constitutive equations can be established, presuming small macroscopic deformations and macroscopic isotropic elastic behaviour. The non-linearity of the material is taken into account by defining Young's modulus as a function of some equivalent strain measure. The parameters in this function will be fitted onto finite element calculations. As applications, a tensile test, a shear test, and a tensile test on a single edge nodged specimen will be discussed.

1 Introduction

1.1 Heterogeneous Materials and Homogenization

Composite materials are used more and more for load carrying components in structures, since their mechanical properties, such as strength, stiffness, and toughness are being improved continuously. On the microscopic level, these materials reveal a structure in which different components can be distinguished. Examples of heterogeneous materials are composites, polymer blends, alloy systems, ceramics, paper, wood and bone. During loading of the material, micromechanical failure mechanisms, such as matrix crazing or cracking, void formation and fibre-matrix debonding, are frequently encountered, which may result in macroscopic so-called *strain softening* behaviour. This is a decreasing stress with increasing strain. The obvious influence of the microscopic deformation on the macroscopic behaviour was shown experimentally for polymer blends by Van der Sanden (1993) and Coomans (1995). The importance of parameters like the average distance between the heterogeneities, the diameter and the spatial distribution of the inclusions appeared to be quite substantial.

When developing new materials, insight in these phenomena is therefore required. Relations between the micromechanical failure mechanisms and the macroscopic deformation behaviour are necessary for predicting macroscopic properties from the microstructure. This will enable the material engineer to adapt the microstructure to obtain the desired mechanical properties, such as high stiffness, strength or toughness. This is called *material design*. Another application of this relation is the *design of structures*. Here, the macroscopic material model (i.e., the constitutive equations), serves as input of a simulation program or an analytical calculation. Complete structures, such as cars and bridges, then can be simulated yielding the desired overall response.

The growing interest in material design has resulted in a increasing demand on robust analytical/numerical procedures for determining macroscopic material properties, relating the microstructural response with the overall macroscopic behaviour. This procedure is called *homogenization* (Vosbeek (1994) and this report, Chapter 2). The homogenization process aims at replacing the structural model with a continuum model that 'best' represents the structural model (Vosbeek 1996). This process can be summarized in the following two steps:

1. the macroscopic state variables (e.g., stresses and strains) have to be defined in terms of those of the microscopic model;
2. the relation between the evolution of the global state and the evolution of the local state has to be determined.

Of course, the second step amounts to determining the constitutive relations.

Regarding the first step, we have to investigate how the continuum state might be defined. To this end, we first define two characteristic length scales: L, the diameter of the (macroscopic) specimen and λ, the characteristic length of the variations of the state of the medium about its average. Now, let us assume that

1. both L and λ are large compared to a distance, a say, within which the material properties undergo considerable variation about their mean value. This is usually referred to as the *separation of scales principle* (Auriault 1991);
2. the character of the variations in an element of size a^3 in one part of the sample is of the same sort as the variations in another part of the sample.

A material that satisfies both these properties, is said to be *statistically homogeneous* (Beran 1968, Vosbeek 1996).

From the second item, it follows that an element of size a^3 can be identified whose mechanical behaviour is representative for the heterogeneous medium as a whole. Such an element is called a *representative volume element*, or short, *RVE*. The first condition now states that a is much smaller than both L and λ. The fact that a is much smaller than L implies that the RVE is small with respect to the medium

as a whole. So, as a first approximation, we neglect its size, associate with each material point an RVE, and identify its state with that of the RVE. The fact that a is much smaller than λ implies that the state does not vary appreciably over the RVE, Fig.1.1(a). The state of a material point of the continuum, s, then can be defined as an appropriate average of the state, $\bar{s}$, of the RVE associated with that point.

In literature, some methods have been proposed to derive models for statistically homogeneous media. Most of these methods are based on elastic, isotropic matrix material behaviour. These models relate the average of the strain to the average of the stress. A large number of analytical micromechanical models have been proposed for predicting the constitutive respons at the macroscopic level. Some of those models are based on so-called self-consistent schemes. These methods provide reasonably good estimates for the overall macroscopic behaviour when the volume fraction of the heterogeneities is low. However, at higher volume fractions, these methods produce substantial discrepancies (e.g. for a cavity, the effective moduli approach zero, for a volume fraction larger than 20%, which is far from realistic). The reason for these discrepancies is importance of the strain gradients (i.e., the variations of the state variables, Fig.1.1(c)). Since these models only use the averages of the strain and the stress as deformation and constitutive variables, respectively, the description becomes inaccurate. In addition, these models are incapable of treating arbitrary distributions of shape, size and location of the heterogeneities, that are frequently encountered in real materials (Ghosh and Moorthy 1995). A more comprehensive overview of these and other methods is given in Nemat-Nasser and Hori (1993) and Mura (1987). Many contributions have been proposed for periodic structures using the asymptotic expansion technique, for elastic solids by Hollister and Kikuchi (1992), Ghosh, Lee, and Moorthy (1995) and Boutin (1996), and for elasto-plastic solids, by Ghosh and Moorthy (1995). The most important drawback of these methods is the assumption of periodicity of the microstructure and the state variables, which obviously will be disturbed in *localization phenomena*, where the separation of scales principle does not hold anymore.

The separation of scales principle can be violated in two different ways. Either a is in the order of the size of the specimen L, in which case a is also in the order of λ, Fig.1.1(b), or $a \ll L$, but the variations of the state s of the RVE are large with respect to the average $\bar{s}$, that is, $a \sim \lambda$, Fig.1.1(c). In the first case, we can no longer associate with each material point an RVE. Instead, each RVE has to be associated with a region of the continuum. Homogenization of this material therefore is inappropriate. In the second case, which is typical for problems dealing with localization phenomena, where large strain gradients occur, we are still allowed to associate with each material point an RVE, but we are not allowed to replace the state of the RVE by its average only. The latter simply does not contain enough information about the actual state of the RVE.

The continuum mechanical description of strain softening materials poses another problem. The constitutive equations used generally obey the principle of local action. It can be shown that these models fail for strain softening (De Borst and Mühlhaus 1991 and (Vosbeek, 1994, Chapter 2)). For instance, Tvergaard and Needleman (1995) show that for shear bands in a local continuum, the post localization behaviour is strongly mesh dependent. An example of an infinite number of solutions

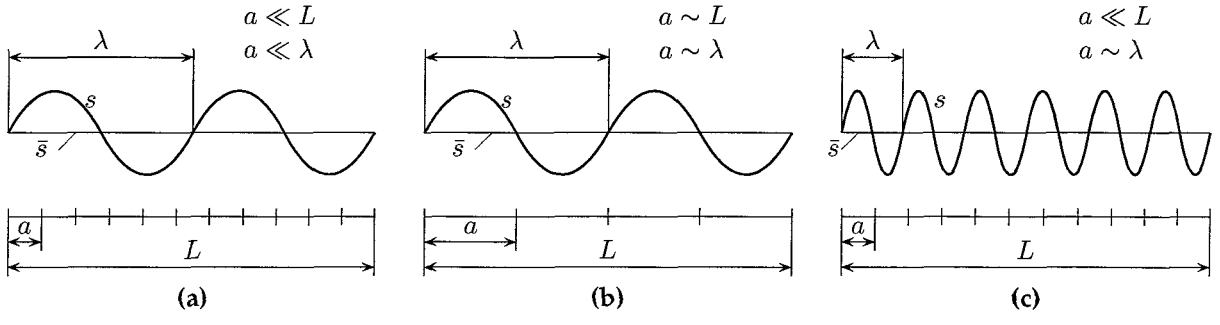

Figure 1.1: A statistically homogeneous medium (a) and two statistically inhomogeneous materials (b) and (c); s represents the value of the state variable and $\bar{s}$ the average of s

when trying to describe strain softening with local models, and mesh dependent solutions, are given in De Borst (1990) and Vosbeek (1994).

A remedy for the problems described above, given by various authors, is that when one allows *long range effects* to enter the constitutive equations, models can be obtained that do have a unique solution, in contrast to local models. One way of including long range effects is to introduce averages of stress and/or strain in the constitutive equations. This leads to non-local models (Tvergaard and Needleman 1995). Another solution is to incorporate partial derivatives of stress and/or strain, leading to *gradient models* (Triantafyllidis and Aifantis 1986). A third way is introducing rotational degrees of freedom in addition to the usual translational degrees of freedom. This leads to *Cosserat continua*.

Hence, a solution is to extend the state of the material point with additional statistical moments of the state of the RVE. The supplementary degrees of freedom of the macroscopic models should be related to these statistical moments. In this report, a Cosserat continuum will be used as a macroscopic material model.

1.2 Scope of the Report

A polycarbonate plate with macroscopic holes is taken as a model-material. As was already mentioned, experiments (i.e., tensile tests) of Coomans (1995) have shown the importance of some parameters like the hole stacking, hole size, hole distribution and strain rate on the mechanical behaviour of the plate. These experimental observations must be investigated in a more mathematical way, by using homogenization techniques and numerical methods.

At this moment, we are already able to carry out numerical simulations, using the finite element method, of the polycarbonate model-material. The material properties are modelled making use of the finite element implementation of the compressible Leonov model (Smit 1994 and Smit and Timmermans 1995). A typical stress-strain curve of this model, using polycarbonate parameters, is depicted in Fig.1.2. However, when the number of holes in the plate is increased, the finite element meshes will become very complex for obtaining accurate results, and, hence, the memory requirements and the CPU-times become infeasable.

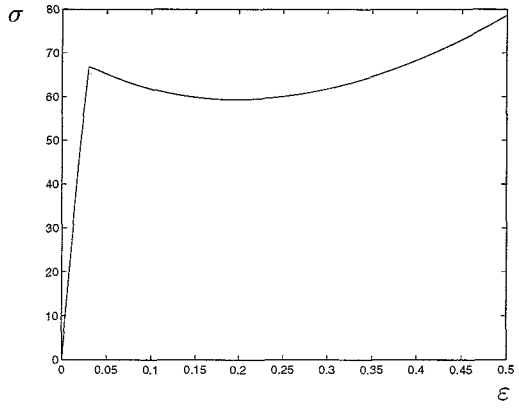

Figure 1.2: A typical stress/strain curve of the compressible Leonov model for polycarbonate parameters

Thus, another way of describing the mechanical behaviour of the perforated plate is desired. In this report, we will use homogenization techniques. First, an RVE has to be defined. Clearly, when the global stacking of the holes is cubic, the RVE is a square with a hole in the centre. A typical result of a tensile test on the RVE are depicted in Fig.1.3. The tensile test is a symmetrical load so only a quarter of the RVE has to be modelled. The undeformed mesh is shown in Fig.1.3(a). The matrix material is modelled according to the compressible Leonov model using polycarbonate parameters. For the hole,

a very soft elastic material is used. On the right edge the displacements are prescribed resulting in a constant strain rate. On the bottom edge the vertical displacements are suppressed, whereas on the left edge the horizontal displacements are zero. Fig.1.3(b) shows the deformed mesh with contourbands of the equivalent Von Mises stress. Here, a white color indicates high stresses, whereas dark colors correspond with low values. The values of the stresses lie between 0 $[MPa]$ and 125 $[MPa]$. It can be concluded that the variations of the state variable in the deformed mesh are of the order of the RVE-size, hence, $a \sim \lambda$, which is analogous to Fig.1.1(c). The resulting load-displacement curve is illustrated in Fig.1.3(c). We may conclude that we have to use homogenization techniques which result in non-local models, because additional statistical moments have to be included.

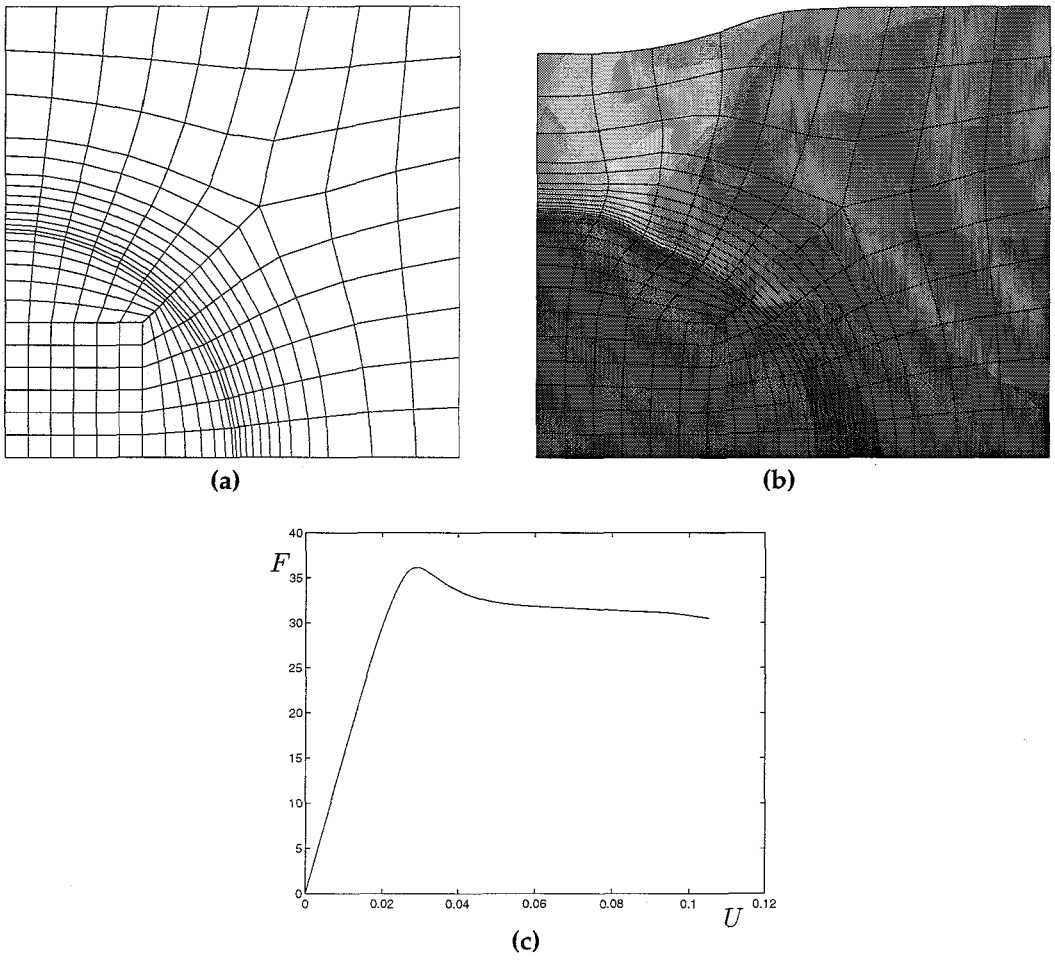

Figure 1.3: (a) The undeformed, (b) the deformed mesh and (c) the resulting force-displacement curve of a tensile test on the RVE

This conclusion led to the use of Cosserat theory at the macroscopic level, which provides rotational degrees of freedom as additional quantities. For simplicity, some assumptions will be made in this report. First of all, we apply a constant strain rate to the RVE. In addition, small macroscopic deformations on account of the used deformation measure and macroscopic isotropic elastic material behaviour on account of the used constitutive equations.

1.3 Outline of the Report

The outline of this report is as follows. In the next Chapter, we will discuss the homogenization procedure. First, for a better understanding, the notion of homogenization, the classical case is discussed. This approach will then be extended to non-local models. Boundary conditions which obey the definitions of the relations between the microscopic and macroscopic state variables, will be devised. Clearly, this can be identified as the first step of the homogenization procedure, as was already discussed. With these boundary conditions, which are applied to the RVE by means of a displacement field, examples are shown which elucidate the influence of the position of the RVE within the macroscopic medium, as well as the influence of the size of the RVE. Finally, an example of a non-local consitutive equation will be formulated, from which it will be made clear that a more heuristical approach in the formulation of the additional degrees of freedom is needed. It is obvious that this is conform the second step of the homogenization process.

Chapter 3 deals with Cosserat mechanics which can be identified as a non-local model. The basic assumptions will be discussed, to gain more insight into the matter. Since the second step of the homogenization will be carried out numerically using the finite element method, a new Cosserat finite element wil be developed. The implementation of the element will be validated on some test problems. Anticipating the strain softening behaviour resulting from the homogenization process of the Leonov model, Fig.1.2, a parameterized function of the E-modulus will be proposed. Some preliminary results are shown to prove the capability of the Cosserat element to describe strain softening, and to show that the element will converge to a unique solution upon mesh refinement.

The homogenization towards Cosserat media will be described in Chapter 4. Actually, this Chapter can be seen as a combination of Chapter 2 and Chapter 3. Again, consistent boundary conditions will be derived, using relations between the local Leonov and global Cosserat deformation terms. The boundary conditions will then be applied to the RVE, which obviously will result in a stress field distribution on the microscopic level. Using a fitting procedure, the parameters used in the function for the E-modulus, are determined which then describe the desired overall constitutive equations. Some results will be shown subsequently.

Finally, in the last Chapter, some conclusions will be drawn and some recommendations will be proposed.

2 Homogenization

As pointed out in the Introduction, classical homogenization methods, which result in local models, are not able to describe localization phenomena properly. In contrast to local models, non-local models are able to describe localization, by including long-range effects in the form of additional degrees of freedom in the constitutive equation. These extra quantities can be explained as being the influence of the neighbourhood on an arbitrary located representative cell.

So, the goal of this homogenization process is to establish a constitutive equation, which, by definition, describes the relation between the macroscopic stresses on one hand and strains and some, yet to be determined, neighbourhood-parameters on the other hand.

In the following, classical homogenization will be elaborated first. After that, this formulation will be extended to non-local models. Using the connection between microscopic and macroscopic deformation quantities (this is the first step of the homogenization process, as has been stated in the Introduction), a so called consistent boundary displacement field is derived. This displacement field, in terms of the macroscopic deformation quantities, will be applied as boundary conditions on the representative volume element. This results in local stresses, which, after averaging, will be applied on the global level. Next, we will use this displacement formulation to give some preliminary results concerning homogenization of a square RVE. Several macroscopic displacement fields are formulated, resulting in a microscopic displacement field on the RVE. In general, this latter field will depend on the RVE-size and the position of the RVE in the continuum. After that, a general non-local constitutive equation will be proposed.

2.1 Classical Homogenization

As was already seen in the Introduction, two levels can be distinguished, i.e. the microscopic, discrete level and the macroscopic, continuum level. The basic assumption here is the existence of an RVE (Fig. 2.1). At the microscopic level, the material is inherently heterogeneous (e.g. inclusions, cracks or, as in our case, holes can be distinguished). Clearly, the RVE is, by definition, also heterogeneous.

Following Vosbeek (1994), the microscopic RVE is supposed to be in equilibrium, that is, if σ_{ij} is the (microscopic) Cauchy stress tensor at position $\boldsymbol{y}$ in the RVE R, associated with point $\mathcal{P}$ at position $\boldsymbol{x}$ in the macroscopic material Ω, we have

$$\frac{\partial \sigma_{ji}(\boldsymbol{x},\boldsymbol{y})}{\partial y_j} = \boldsymbol{0}, \qquad \boldsymbol{y} \in R, \quad \boldsymbol{x} \in \Omega. \tag{2.1}$$

Furthermore, the material behaviour in the RVE is assumed to be known in the form of a microscopic constitutive equation, by which the relation between the stress tensor $\boldsymbol{\sigma}$ and the, yet to be defined, strain tensor $\boldsymbol{\varepsilon}$ is established,

$$\boldsymbol{\sigma}(\boldsymbol{x},\boldsymbol{y}) \sim \boldsymbol{\varepsilon}(\boldsymbol{x},\boldsymbol{y}), \qquad \boldsymbol{y} \in R. \tag{2.2}$$

A set of boundary conditions must be provided to complete the mechanical problem for the RVE. These boundary conditions usually take the form of prescribed displacements and/or tractions.

The macroscopic degrees of freedom are defined as averages of the microscopic corresponding quantities,

$$\bar{\boldsymbol{\sigma}}(\boldsymbol{x}) = \langle \boldsymbol{\sigma} \rangle (\boldsymbol{x}) \qquad \text{and} \qquad \bar{\boldsymbol{\varepsilon}}(\boldsymbol{x}) = \langle \boldsymbol{\varepsilon} \rangle (\boldsymbol{x}). \tag{2.3}$$

The average of some arbitrary function $\phi(\boldsymbol{x},\boldsymbol{y})$ over the region R, occupied by the RVE, is defined by:

$$\langle \phi \rangle (\boldsymbol{x}) \equiv \frac{1}{V} \int_R \phi(\boldsymbol{x},\boldsymbol{y}) \, \mathrm{d}\boldsymbol{y} \qquad \text{with} \qquad V = \int_R \mathrm{d}\boldsymbol{y} \tag{2.4}$$

The definitions of the stress and strain quantities yield the formulation of the boundary conditions on the RVE. To put it in other words, the boundary conditions will be formulated in terms of these macroscopic degrees of freedom.

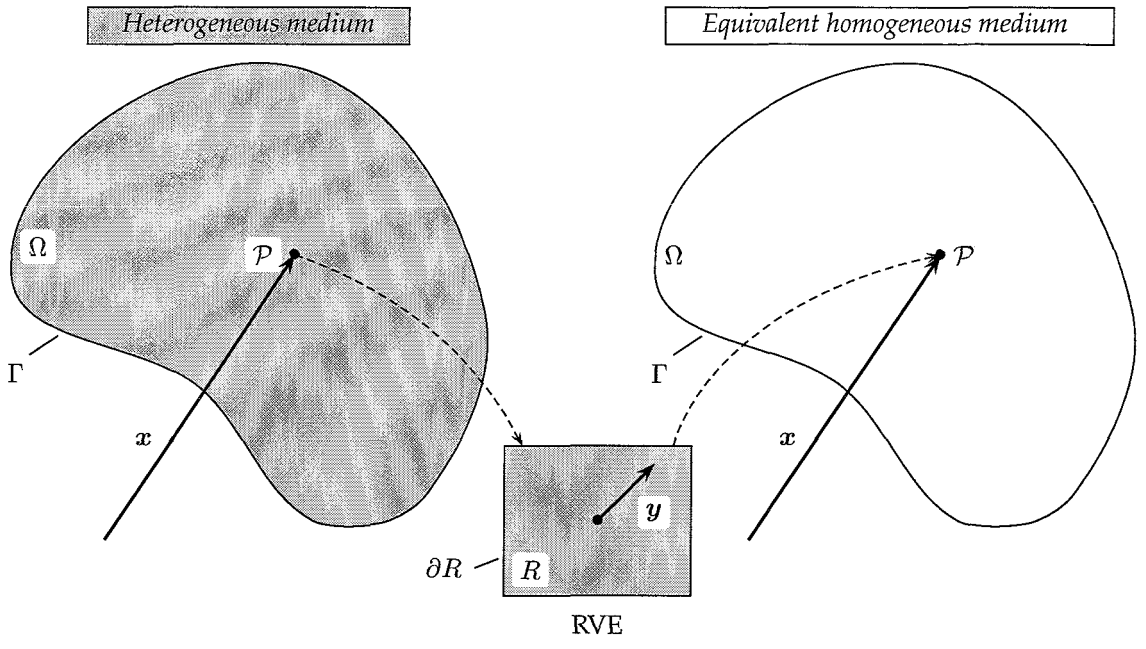

Figure 2.1: Graphical representation of the RVE

2.1.1 Derivation of the Consistent Boundary Conditions

The applied boundary conditions may not be chosen randomly, but they must be consistent with (2.3). In this Section, consistent conditions will be derived. First, we use the chain rule and the equilibrium of the RVE, i.e. (2.1), to get the following expression:

$$\frac{\partial}{\partial y_k}(\sigma_{ik}y_j) = \frac{\partial \sigma_{ik}}{\partial y_k}y_j + \sigma_{ij} \overset{(2.1)}{=} \sigma_{ij}. \tag{2.5}$$

Integration this equation over R, applying Gauß' divergence theorem and taking into account the symmetry of the stress tensor, yields the consistency relations for the boundary load vector $\boldsymbol{p}$:

$$\bar{\sigma}_{ij}(\boldsymbol{x}) = \frac{1}{2V}\int_{\partial R}\left(p_i(\boldsymbol{x},\boldsymbol{y})y_j + p_j(\boldsymbol{x},\boldsymbol{y})y_i\right)\,\mathrm{d}s, \tag{2.6}$$

where $\boldsymbol{p}(\boldsymbol{x},\boldsymbol{y}) = \boldsymbol{\sigma}(\boldsymbol{x},\boldsymbol{y})\boldsymbol{n}(\boldsymbol{x},\boldsymbol{y})$ with $\boldsymbol{n}(\boldsymbol{x},\boldsymbol{y})$ is the outward normal on ∂R.

To find consistent kinematical boundary conditions, we assume a definition of the used strain quantity, viz. the linear strain tensor which is defined as:

$$\varepsilon_{ij}(\boldsymbol{x},\boldsymbol{y}) = \frac{1}{2}\left(\frac{\partial u_i(\boldsymbol{x},\boldsymbol{y})}{\partial x_j} + \frac{\partial u_j(\boldsymbol{x},\boldsymbol{y})}{\partial x_i}\right). \tag{2.7}$$

Again, integrating this equation and using Gauß' divergence theorem on (2.7), we obtain the consistency relations for the boundary displacements,

$$\bar{\varepsilon}_{ij}(\boldsymbol{x}) = \frac{1}{2V}\int_{\partial R}\left(u_i(\boldsymbol{x},\boldsymbol{y})n_j(\boldsymbol{x},\boldsymbol{y}) + u_j(\boldsymbol{x},\boldsymbol{y})n_i(\boldsymbol{x},\boldsymbol{y})\right)\,\mathrm{d}s. \tag{2.8}$$

Simple dynamical boundary conditions that satisfy (2.6) are uniform tractions,

$$\boldsymbol{p}_0(\boldsymbol{x},\boldsymbol{y}) = \bar{\boldsymbol{\sigma}}(\boldsymbol{x})\boldsymbol{n}(\boldsymbol{x},\boldsymbol{y}), \qquad \boldsymbol{y} \in \partial R. \tag{2.9}$$

The most simple kinematical boundary conditions which satisfy (2.8) are linear displacement fields (i.e., uniform strain fields),

$$\boldsymbol{u}_0(\boldsymbol{x},\boldsymbol{y}) = \bar{\boldsymbol{\varepsilon}}(\boldsymbol{x})\boldsymbol{y}, \qquad \boldsymbol{y} \in \partial R. \tag{2.10}$$

Examples of the above consistent boundary conditions are illustrated in Fig. 2.2.

Attention will now be focussed on non-local models, which, as has already been discussed, are required to describe localization behaviour properly.

2.2 Non-Local Models

Classical homogenization can be applied when the separation of scales between the microscopic and macroscopic levels is good, i.e. $a/L \ll 1$, where a is some characteristic microscopic size-parameter, and L its macroscopic equivalent. For localization phenomena, $a/L \not\ll 1$, hence classical homogenization fails. Thus, we need so-called *non-local models* where the ratio a/L is taken as a *material parameter* for the macroscopic constitutive equation. The term non-local represents the contribution from field quantities in the neighbourhood of that point (long-range effects).

In these non-local constitutive equations, additional degrees of freedom are introduced to describe the deformation state. Also, an internal length scale must be present in the description of the material. In this Section, the additional quantities of the macroscopic degrees of freedom are first and second order partial derivatives of the strain field. Derivatives of the macroscopic stress field are not taken into account, as in that case one requires additional equilibrium equations, which are not trivial to formulate. So, the macroscopic degrees of freedom at this point are the stress field $\bar{\boldsymbol{\sigma}}(\boldsymbol{x})$, the strain field $\bar{\boldsymbol{\varepsilon}}(\boldsymbol{x})$ and first and second order partial derivatives of this strain field. Assuming ergodicity, these derivatives are defined in terms of their corresponding microscopic quantities:

$$\frac{\partial \bar{\varepsilon}_{ij}(\boldsymbol{x})}{\partial x_k} = \frac{1}{V}\int_R \frac{\partial \varepsilon_{ij}(\boldsymbol{x},\boldsymbol{y})}{\partial y_k}\,\mathrm{d}\boldsymbol{y} = \frac{1}{V}\int_{\partial R} \varepsilon_{ij}(\boldsymbol{x},\boldsymbol{y}) n_k(\boldsymbol{x},\boldsymbol{y})\,\mathrm{d}s, \tag{2.11}$$

$$\frac{\partial^2 \bar{\varepsilon}_{ij}(\boldsymbol{x})}{\partial x_k \partial x_l} = \frac{1}{V}\int_R \frac{\partial^2 \varepsilon_{ij}(\boldsymbol{x},\boldsymbol{y})}{\partial y_k \partial y_l}\,\mathrm{d}\boldsymbol{y} = \frac{1}{V}\int_{\partial R} \frac{\partial \varepsilon_{ij}(\boldsymbol{x},\boldsymbol{y})}{\partial y_k} n_l(\boldsymbol{x},\boldsymbol{y})\,\mathrm{d}s. \tag{2.12}$$

Here, the second equal-sign represents the application of the divergence theorem. It should also be noted that only first and second order derivatives of the strain field are taken into account. The consistency demands on the dynamical conditions remain the same, i.e. (2.6). But, for the kinematical boundary conditions, not only (2.8) must be satisfied, but also (2.11) and (2.12). Clearly, from these demands, the displacement field cannot be linear anymore, but must at least be cubic, or even of higher order. In the following, a consistent boundary displacement field is derived which obeys the demands (2.8), (2.11) and (2.12).

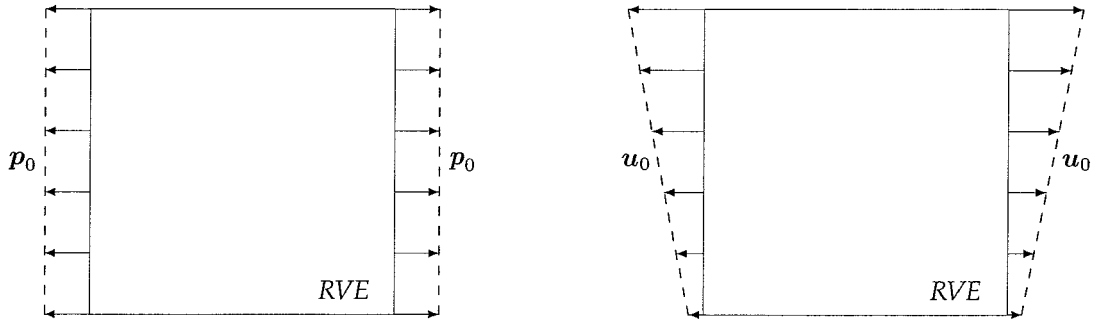

Figure 2.2: Prescribed consistent boundary conditions

2.2.1 Derivation of a Consistent Displacement Field

To derive a displacement field, one can expand a general field into a Taylor series around the origin of the RVE $\boldsymbol{y} = \mathbf{0}$, disregarding the terms of order $\mathcal{O}(\|\boldsymbol{y}\|^4)$, and keeping $\boldsymbol{x}$ constant,

$$\begin{aligned} u_i(\boldsymbol{x},\boldsymbol{y}) &= u_{0i}(\boldsymbol{x}) + \frac{\partial u_i(\boldsymbol{x},\boldsymbol{y})}{\partial y_j}\bigg|_{\boldsymbol{y}=\mathbf{0}} y_j + \frac{1}{2}\frac{\partial^2 u_i(\boldsymbol{x},\boldsymbol{y})}{\partial y_j \partial y_k}\bigg|_{\boldsymbol{y}=\mathbf{0}} y_j y_k + \frac{1}{6}\frac{\partial^3 u_i(\boldsymbol{x},\boldsymbol{y})}{\partial y_j \partial y_k \partial y_l}\bigg|_{\boldsymbol{y}=\mathbf{0}} y_j y_k y_l \\ &= u_{0i}(\boldsymbol{x}) + \alpha_{ij}(\boldsymbol{x}) y_j + \frac{1}{2}\beta_{ijk}(\boldsymbol{x}) y_j y_k + \frac{1}{6}\gamma_{ijkl}(\boldsymbol{x}) y_j y_k y_l, \qquad \boldsymbol{y} \in R. \end{aligned} \tag{2.13}$$

Applying the definition of the strain tensor according to (2.7), and assuming symmetry conditions $\alpha_{ij} = \alpha_{ji}$, $\beta_{ijk} = \beta_{jik} = \beta_{ikj}$, $\gamma_{ijkl} = \gamma_{jikl} = \gamma_{iljk} = \gamma_{iklj}$, yields

$$\varepsilon_{ij}(\boldsymbol{x},\boldsymbol{y}) = \alpha_{ij}(\boldsymbol{x}) + \beta_{ijk}(\boldsymbol{x}) y_k + \frac{1}{2}\gamma_{ijkl}(\boldsymbol{x}) y_k y_l, \tag{2.14}$$

$$\frac{\partial \varepsilon_{ij}(\boldsymbol{x},\boldsymbol{y})}{\partial y_k} = \beta_{ijk}(\boldsymbol{x}) + \gamma_{ijkl}(\boldsymbol{x}) y_l, \tag{2.15}$$

$$\frac{\partial^2 \varepsilon_{ij}(\boldsymbol{x},\boldsymbol{y})}{\partial y_k \partial y_l} = \gamma_{ijkl}(\boldsymbol{x}). \tag{2.16}$$

To determine the corresponding macroscopic degrees of freedom of the above quantities, we apply (2.4) to get

$$\begin{aligned} \bar{u}_i(\boldsymbol{x}) &= \frac{1}{V}\int_R u_i(\boldsymbol{x},\boldsymbol{y})\,\mathrm{d}\boldsymbol{y} \\ &= u_{0i}(\boldsymbol{x}) + \alpha_{ij}(\boldsymbol{x}) M_j^{(1)} + \frac{1}{2}\beta_{ijk}(\boldsymbol{x}) M_{jk}^{(2)} + \frac{1}{6}\gamma_{ijkl}(\boldsymbol{x}) M_{jkl}^{(3)}, \end{aligned} \tag{2.17}$$

$$\bar{\varepsilon}_{ij}(\boldsymbol{x}) = \frac{1}{V}\int_R \varepsilon_{ij}(\boldsymbol{x},\boldsymbol{y})\,\mathrm{d}\boldsymbol{y} = \alpha_{ij}(\boldsymbol{x}) + M_k^{(1)}\beta_{ijk}(\boldsymbol{x}) + \frac{1}{2}M_{kl}^{(2)}\gamma_{ijkl}(\boldsymbol{x}), \tag{2.18}$$

$$\frac{\partial \bar{\varepsilon}_{ij}(\boldsymbol{x})}{\partial x_k} = \frac{1}{V}\int_R \frac{\partial \varepsilon_{ij}(\boldsymbol{x},\boldsymbol{y})}{\partial y_k}\,\mathrm{d}\boldsymbol{y} = \beta_{ijk}(\boldsymbol{x}) + M_l^{(1)}\gamma_{ijkl}(\boldsymbol{x}), \tag{2.19}$$

$$\frac{\partial^2 \bar{\varepsilon}_{ij}(\boldsymbol{x})}{\partial x_k \partial x_l} = \frac{1}{V}\int_R \frac{\partial^2 \varepsilon_{ij}(\boldsymbol{x},\boldsymbol{y})}{\partial y_k \partial y_l}\,\mathrm{d}\boldsymbol{y} = \gamma_{ijkl}(\boldsymbol{x}), \tag{2.20}$$

where

$$M_i^{(1)} = \frac{1}{V}\int_R y_i\,\mathrm{d}\boldsymbol{y}, \tag{2.21}$$

$$M_{ij}^{(2)} = \frac{1}{V}\int_R y_i y_j\,\mathrm{d}\boldsymbol{y}, \tag{2.22}$$

$$M_{ijk}^{(3)} = \frac{1}{V}\int_R y_i y_j y_k\,\mathrm{d}\boldsymbol{y}. \tag{2.23}$$

Note that in the case of a prescribed linear displacement field, (2.10), $\alpha_{ij}(\boldsymbol{x})$ equals $\bar{\varepsilon}_{ij}(\boldsymbol{x})$, and subsequently both $\beta_{ijk}(\boldsymbol{x})$ and $\gamma_{ijkl}(\boldsymbol{x})$ vanish.

Because we need explicit expressions for α_{ij}, β_{ijk}, γ_{ijkl} and u_{0i}, we have to invert the above relations:

$$\begin{aligned}
\gamma_{ijkl}(\boldsymbol{x}) &= \frac{\partial^2 \bar{\varepsilon}_{ij}(\boldsymbol{x})}{\partial x_k \partial x_l}, \\
\beta_{ijk}(\boldsymbol{x}) &= \frac{\partial \bar{\varepsilon}_{ij}(\boldsymbol{x})}{\partial x_k} - M_l^{(1)} \frac{\partial^2 \bar{\varepsilon}_{ij}(\boldsymbol{x})}{\partial x_k \partial x_l}, \\
\alpha_{ij}(\boldsymbol{x}) &= \bar{\varepsilon}_{ij}(\boldsymbol{x}) - M_k^{(1)} \frac{\partial \bar{\varepsilon}_{ij}(\boldsymbol{x})}{\partial x_k} + M_k^{(1)} M_l^{(1)} \frac{\partial^2 \bar{\varepsilon}_{ij}(\boldsymbol{x})}{\partial x_k \partial x_l} - \frac{1}{2} M_{kl}^{(2)} \frac{\partial^2 \bar{\varepsilon}_{ij}(\boldsymbol{x})}{\partial x_k \partial x_l}, \\
u_{0i}(\boldsymbol{x}) &= \bar{u}_i(\boldsymbol{x}) - \bar{\varepsilon}_{ij}(\boldsymbol{x}) M_j^{(1)} + \Big[M_j^{(1)} M_k^{(1)} - \frac{1}{2} M_{jk}^{(2)} \Big] \frac{\partial \bar{\varepsilon}_{ij}(\boldsymbol{x})}{\partial x_k} \\
&\quad + \Big[\frac{1}{2} M_j^{(1)} M_{kl}^{(2)} - M_j^{(1)} M_k^{(1)} M_l^{(1)} + \frac{1}{2} M_{jk}^{(2)} M_l^{(1)} - \frac{1}{6} M_{jkl}^{(3)} \Big] \frac{\partial^2 \bar{\varepsilon}_{ij}(\boldsymbol{x})}{\partial x_k \partial x_l}.
\end{aligned}$$

Now, we substitute these quantities in expression (2.13), yielding the *general displacement field* at the boundary on the RVE,

$$\begin{aligned}
u_i(\boldsymbol{x}, \boldsymbol{y}) &= \bar{u}_{0i}(\boldsymbol{x}) + \bar{\varepsilon}_{ij}(\boldsymbol{x})[y_j - M_j^{(1)}] + \frac{1}{2}\Big[y_j y_k - 2 y_j M_k^{(1)} + 2 M_j^{(1)} M_k^{(1)} - M_{jk}^{(2)} \Big] \frac{\partial \bar{\varepsilon}_{ij}(\boldsymbol{x})}{\partial x_k} \\
&\quad + \frac{1}{6}\Big[y_j y_k y_l - 3 y_j y_k M_l^{(1)} + 6 y_j M_k^{(1)} M_l^{(1)} - 3 y_j M_{kl}^{(2)} - 6 M_j^{(1)} M_k^{(1)} M_l^{(1)} \\
&\quad + 3 M_j^{(1)} M_{kl}^{(2)} + 3 M_{jk}^{(2)} M_l^{(1)} - M_{jkl}^{(3)} \Big] \frac{\partial^2 \bar{\varepsilon}_{ij}(\boldsymbol{x})}{\partial x_k \partial x_l}, \quad \boldsymbol{y} \in \partial R.
\end{aligned} \tag{2.24}$$

Obviously, the constants $M_i^{(1)}$, $M_{ij}^{(2)}$ and $M_{ijk}^{(3)}$ are geometry parameters, and as such can be calculated. As an example, we take a two-dimensional, square RVE, i.e. $y_1, y_2 \in [-a, a]$. Consequently, we are able to calculate the constants:

$$\begin{pmatrix} M_1^{(1)} \\ M_2^{(1)} \end{pmatrix} = \frac{1}{4a^2} \int_{-a}^{a} \int_{-a}^{a} \begin{pmatrix} y_1 \\ y_2 \end{pmatrix} \mathrm{d}y_1 \mathrm{d}y_2 = \boldsymbol{0}, \tag{2.25}$$

$$\begin{pmatrix} M_{11}^{(2)} & M_{12}^{(2)} \\ M_{21}^{(2)} & M_{22}^{(2)} \end{pmatrix} = \frac{1}{4a^2} \int_{-a}^{a} \int_{-a}^{a} \begin{pmatrix} y_1^2 & y_1 y_2 \\ y_2 y_1 & y_2^2 \end{pmatrix} \mathrm{d}y_1 \mathrm{d}y_2 = \frac{1}{3} a^2 \boldsymbol{I}, \tag{2.26}$$

where $\boldsymbol{I}$ is the unity-tensor, with components δ_{kl}, being Kronecker's delta. Because the integrand of $M_i^{(1)}$ is anti-symmetric in both y_1 as well as y_2, and the RVE is symmetric in this coordinate system, we can deduce that $M_{ijk}^{(3)} = \boldsymbol{0}$. Substituting these values in (2.24), we obtain the *displacement field for a square RVE*:

$$\begin{aligned}
u_i(\boldsymbol{x}, \boldsymbol{y}) &= \bar{u}_{0i}(\boldsymbol{x}) + \bar{\varepsilon}_{ij}(\boldsymbol{x}) y_j + \frac{1}{2}\Big[y_j y_k - \frac{1}{3} a^2 \delta_{jk} \Big] \frac{\partial \bar{\varepsilon}_{ij}(\boldsymbol{x})}{\partial x_k} \\
&\quad + \frac{1}{6}\Big[y_j y_k y_l - y_j \delta_{kl} a^2 \Big] \frac{\partial^2 \bar{\varepsilon}_{ij}(\boldsymbol{x})}{\partial x_k \partial x_l} y_j, \quad \boldsymbol{y} \in \partial R.
\end{aligned} \tag{2.27}$$

This equation is written out in Appendix A.

It can be concluded that the displacement field is a function of the chosen position of the RVE within the macroscopic medium. Choosing the position ($\boldsymbol{x}$), results in the determination of the parameters $\bar{\varepsilon}_{ij}$, $\partial \bar{\varepsilon}_{ij} / \partial x_k$ and $\partial^2 \bar{\varepsilon}_{ij} / \partial x_k \partial x_l$. Consequently, the RVE-size a characterizes the micro-scale of the coordinates $\boldsymbol{y}$.

To determine the effect of the a-size in advance, we will use a dimensionless form of the displacement field (2.27). Therefore, we introduce the dimensionless parameters, $\boldsymbol{\xi} = \boldsymbol{x}/L$ and $\boldsymbol{\eta} = \boldsymbol{y}/a$, from which

it follows that

$$\frac{u_i(\boldsymbol{x},\boldsymbol{y})}{a} = \frac{\bar{u}_{0i}(\boldsymbol{x})}{a} + \bar{\varepsilon}_{ij}\eta_j + \frac{1}{2}\left(\frac{a}{L}\right)\left[\eta_j\eta_k - \frac{1}{3}\delta_{jk}\right]\frac{\partial\bar{\varepsilon}_{ij}}{\partial\xi_k} + \frac{1}{6}\left(\frac{a}{L}\right)^2\left[\eta_j\eta_k\eta_l - \eta_j\delta_{kl}\right]\frac{\partial^2\bar{\varepsilon}_{ij}}{\partial\xi_k\partial\xi_l}, \quad \boldsymbol{\eta}\in[-1,1]^2 \tag{2.28}$$

From this equation, it's easily seen that, when reducing the ratio a/L, the higher order terms vanish gradually. So, a linear relation emanates from this, which is surely equal to the classical result (2.10).

In Appendix B, some results are shown regarding the effect of the size and position of the RVE on the boundary fields, which will be applied on the edge of the RVE. First, two arbitrary displacement fields are postulated. From these examples, the influence of higher order gradients in relation to the RVE size and position will become more clear. Later on, the attention is been focussed on a more practical situation: a displacement field near a crack tip.

2.3 A Non-Local Constitutive Equation

The second step of the homogenization procedure implies the derivation of the relation between the kinematical and the dynamical quantities, i.e., the strains and the stresses, respectively, see the discussion in the Introduction. This relation is governed by the equilibrium of the RVE, the local constitutive equations, the boundary conditions applied on the RVE and the relation between the microscopic and macroscopic quantities.

Two different approaches can be distinguished,

- multi level method:
  given a macroscopic deformation state, appropriate boundary conditions are applied on the microscopic cell. This will result in local stresses, after which global stresses over the RVE can be obtained. This procedure will be computationally expensive, since after each increment, a new simulation has to be started.
- deriving a closed form constitutive equation:
  - analytical: considering the strongly non-linear and time-dependent local material behaviour, this is likely to be difficult;
  - expanding each stress component in a Taylor series: assuming the stress being a function of the strain and some of its gradients, the stress can be expanded in a Taylor series, and the coefficients appearing in this relation have to be determined, e.g. by fitting. Below, this method will be discussed briefly.
  - choosing a more heuristical approach in the formulation of the constitutive equations, will greatly reduce computational times. This method will be elaborated in the next Chapter.

To obtain a (macroscopic) non-local constitutive equations, we assume that the stress $\bar{\sigma}_{ij}$ is a function of the strain $\bar{\varepsilon}_{kl}$ and the Laplacian of the strain $\Delta\bar{\varepsilon}_{kl}$. This function $f_{ij}(\bar{\varepsilon}_{kl},\Delta\bar{\varepsilon}_{kl})$ may accordingly be expanded in a Taylor series round $(\bar{\varepsilon}_{kl},\Delta\bar{\varepsilon}_{kl}) = (\mathbf{0},\mathbf{0})$, obtaining

$$\begin{aligned}\bar{\sigma}_{ij} &= f_{ij}(\bar{\varepsilon}_{kl},\Delta\bar{\varepsilon}_{kl})\\ &= f_{ij}(\mathbf{0},\mathbf{0}) + A_{ijkl}\bar{\varepsilon}_{kl} + B_{ijkl}\Delta\bar{\varepsilon}_{kl} + \frac{1}{2}C_{ijklmn}\bar{\varepsilon}_{kl}\bar{\varepsilon}_{mn}\\ &\quad + \frac{1}{2}D_{ijklmn}\Delta\bar{\varepsilon}_{kl}\Delta\bar{\varepsilon}_{mn} + E_{ijklmn}\bar{\varepsilon}_{kl}\Delta\bar{\varepsilon}_{mn} + \mathcal{O}(\|\bar{\varepsilon}_{kl}\|^3,\|\Delta\bar{\varepsilon}_{kl}\|^3).\end{aligned}$$

Because a strainless state may not result in stresses, it follows that $f_{ij}(\mathbf{0},\mathbf{0}) = \mathbf{0}$. For the two-dimensional case, and assuming symmetry of the strain, that is, $\bar{\varepsilon}_{12} = \bar{\varepsilon}_{21}$ and $\Delta\bar{\varepsilon}_{12} = \Delta\bar{\varepsilon}_{21}$, we then have the following for each stress component. The number of constants in A_{ijkl} is three, in B_{ijkl} also three, in

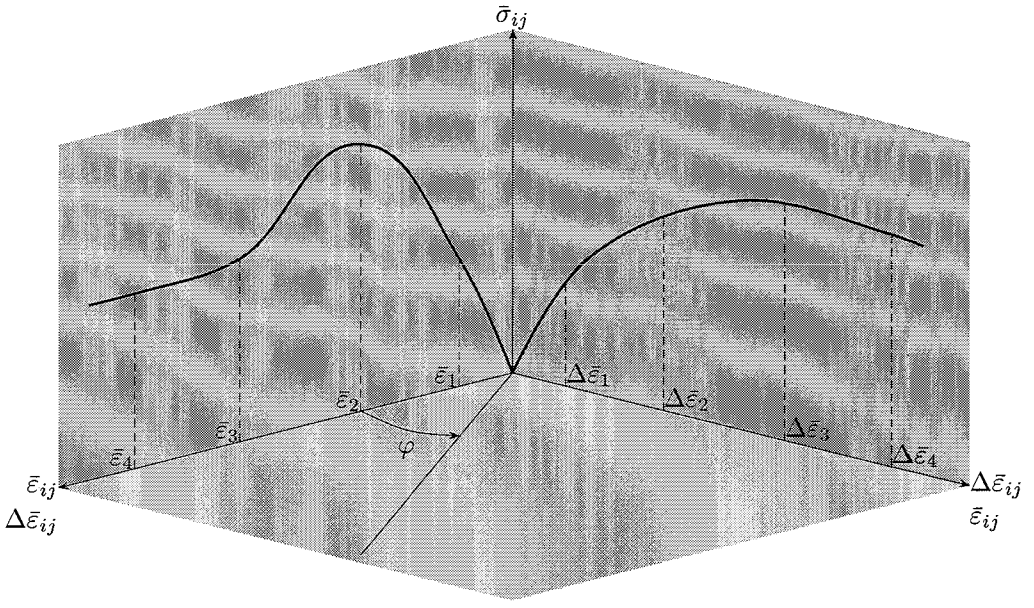

Figure 2.3: Graphical representation of a stress component $\bar{\sigma}_{ij}$ as a function of both a strain component $\bar{\varepsilon}_{ij}$ as well as a component of the Laplacian of the strain $\Delta\bar{\varepsilon}_{ij}$

C_{ijklmn} six, in D_{ijklmn} also six, and, finally, in E_{ijklmn} nine. Thus, the total number of constants which have to be determined, that is, the number of constants for one stresscomponent, is 27. In Fig.2.3, the above is illustrated graphically. Note that this surface, which only is represented by the cutting lines in the corresponding planes, is depicted for one stress component. The procedure will be as follows. The angle φ may be chosen incrementally (e.g. four values between 0 and 90 degrees). Then, for a fixed angle, several combinations of $\bar{\varepsilon}_{ij}$ and $\Delta\bar{\varepsilon}_{ij}$ must be taken. As an example, for a certain value of φ, the combinations are depicted as $\bar{\varepsilon}_i$–$\Delta\bar{\varepsilon}_i$ for $i = 1, \ldots, 4$. These strain combinations are then applied on the RVE, by means of the displacement field, which is a function of these strain quantities, as was discussed in the previous Section. From this, a surface can be fitted for each stress component. This surface then represents a constitutive equation. In principle, when 27 independent simulations are done, the constants for each stress component may be derived. However, we may assume that the surface in the six dimensional space, that is, the $(\bar{\varepsilon}_{11}, \bar{\varepsilon}_{22}, \bar{\varepsilon}_{12}, \Delta\bar{\varepsilon}_{11}, \Delta\bar{\varepsilon}_{22}, \Delta\bar{\varepsilon}_{12},)$–space, is irregular, so when making 27 other simulations, the constants may very well be different from the first set obtained. To overcome this problem, a least squares fitting procedure will have to be used to determine the constants. A reasonable estimate for the number of divisions of an axis, e.g. in Fig.2.3 this number is four, will be ten, although this is, at this point, quite arbitrary. Then the number of simulations, when using the aforementioned least squares fitting procedure in the six dimenional space, will be 10^6. This is quite large, for one stress component. Because this method then reduces to an ordinary fitting problem, and the insight gained using this method is negligible, we further abandon this procedure.

3 Cosserat Theory

In the Introduction, it was stated that non-local models are able to describe strain softening, by allowing long-range effects to enter the constitutive equations. One way to include these effects is to introduce averages of stress and/or strain. Another solution is to incorporate partial derivatives of stress and/or strain, leading to the so-called gradient models. In this work, however, we look at yet another possibility which results in non-local models by introducing rotational degrees of freedom, which leads to a so-called *Cosserat continuum*.

In classical continuum mechanics, a material point has three degrees of freedom: the displacements in three independent directions. Different displacements of two neighbouring points result in a deformation of the material, Fig.3.1(a). This deformation then can be characterised by three normal strains and three shear strains, assuming symmetry of the strain tensor.

In Cosserat theory, a material point has six degrees of freedom, viz. three translational degrees of freedom (the displacements in three independent directions), and three rotational degrees of freedom (the rotations around three independent axes). The deformation is not only characterized by the difference in displacements of the two neighbouring bodies, resulting in normal and shear strains, but also by the difference in rotations, resulting in so-called *curvatures*, Fig.3.1(b). This will be exemplified in the next Section.

To determine the constitutive equations, we will use a homogenization process which uses the local microscopic properties of the material for the macroscopic constitutive behaviour (Fig. 3.2). The deformation of the macroscopic continuum will be applied on the RVE by means of appropriate boundary conditions. The deformation caused by these boundary conditions will result in a stress field in the RVE, which will be applied on the global level, after an appropriate averaging process. This homogenization procedure will be carried out numerically in the next Chapter, using the finite element method at the microscopic and the macroscopic level. Since we apply Cosserat mechanics on the global level, a new macroscopic finite element must be defined. This element will be tested on its capability, in conjunction with the Leonov-model at the microscopic level, to provide a proper description of the macroscopic material behaviour.

First, we give a concise overview of Cosserat mechanics, which can be found in a more comprehensive form in Nowacki (1986). Next, the formulation of the new element will be elaborated. Finally, the performance of this element will be validated on some test problems.

3.1 General Theory

As a starting point, we will give the balance laws of moment and moment of momentum, for both the classical continuum mechanics case as well as the Cosserat case. This comparison will be illuminating for understanding Cosserat mechanics.

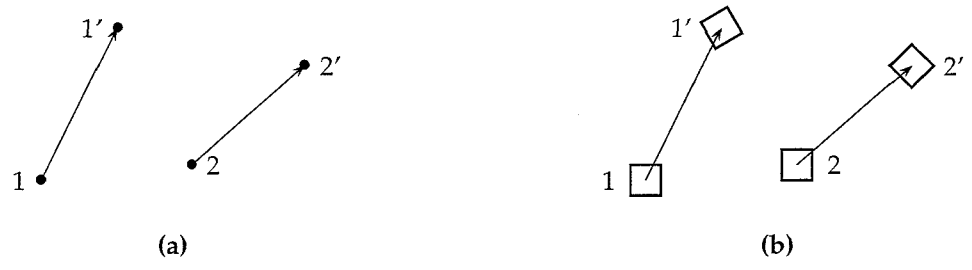

Figure 3.1: Classical mechanics deformation (a) and Cosserat mechanics deformation (b)

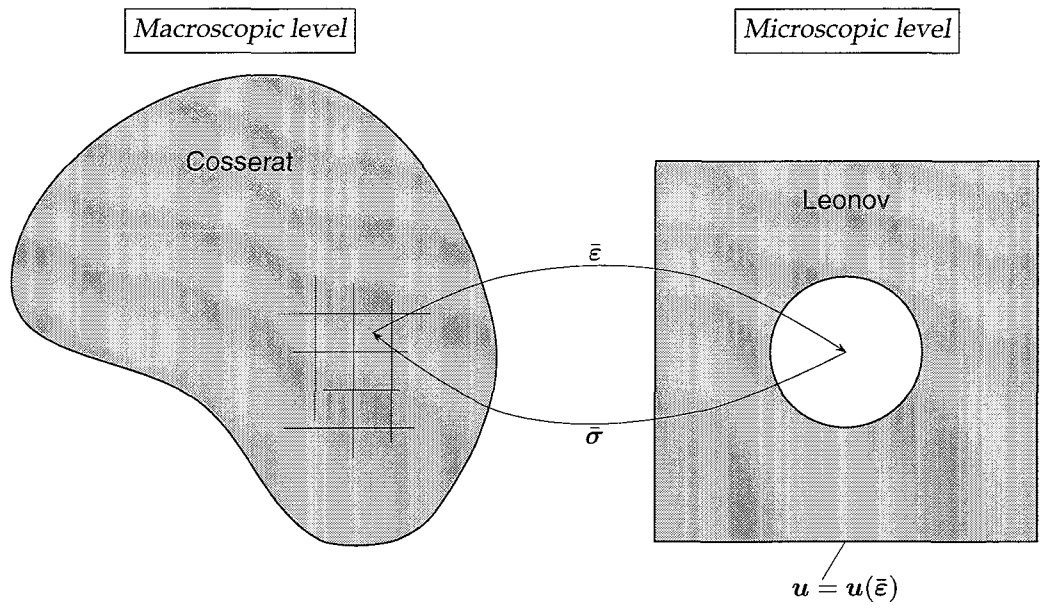

Figure 3.2: Schematic representation of the homogenization procedure. The global strain field $\bar{\varepsilon}$ results in boundary conditions $\boldsymbol{u}(\bar{\varepsilon})$, which lead to stresses on the RVE. After an appropriate averaging process, yielding the global stresses $\bar{\sigma}$, these stresses will be applied on the macroscopic level.

Classical Continuum Mechanics Approach

Consider a material body that occupies a bounded region R. Each point can be identified with a position vector $\boldsymbol{x}$. The displacements of a point in that body are given by a displacement vector $\boldsymbol{u}$ while the strain tensor is defined as $\varepsilon_{ij} = (\partial u_i/\partial x_j + \partial u_j/\partial x_i)/2$. External loads are represented by a stress vector $\boldsymbol{t}$, defined on the boundary ∂r of the region r, which is an arbitrary subdomain of R, and by a volume load vector $\boldsymbol{b}$, defined on r (Fig.3.3(a)). The physical dimension of $\boldsymbol{t}$ is force per unit area, whereas the dimension of $\boldsymbol{b}$ equals force per unit volume. For each subdomain r, the quasi-static force and moment balance equations can then be written as, respectively,

$$\int_{\partial r} \boldsymbol{t}\, \mathrm{d}s + \int_{r} \boldsymbol{b}\, \mathrm{d}\boldsymbol{x} = \boldsymbol{0}, \qquad \text{and} \qquad \int_{\partial r} (\boldsymbol{x} \times \boldsymbol{t})\, \mathrm{d}s + \int_{r} (\boldsymbol{x} \times \boldsymbol{b})\, \mathrm{d}\boldsymbol{x} = \boldsymbol{0}. \tag{3.1}$$

According to Cauchy, the stress vector $\boldsymbol{t}$ is assumed to depend continuously upon $\boldsymbol{n}$, the outward normal to ∂r, i.e., $t_i = \sigma_{ji} n_j$. Substituting Cauchy and using Gauß' divergence theorem, we get for the force balance equations

$$\int_{\partial r} \sigma_{ji} n_j \, \mathrm{d}s + \int_{r} b_i \, \mathrm{d}\boldsymbol{x} = \boldsymbol{0} \quad \rightarrow \quad \int_{r} \left(\frac{\partial \sigma_{ji}}{\partial x_j} + b_i \right) \mathrm{d}\boldsymbol{x} = \boldsymbol{0} \quad \xrightarrow{\forall r} \quad \frac{\partial \sigma_{ji}}{\partial x_j} + b_i = \boldsymbol{0} \quad \text{in } R, \tag{3.2}$$

and, when applying Cauchy for the moment balance equations, we get

$$\int_{\partial r} \epsilon_{ijk} x_j \sigma_{lk} n_l \, \mathrm{d}s + \int_{r} \epsilon_{ijk} x_j b_k \, \mathrm{d}\boldsymbol{x} = \boldsymbol{0}, \tag{3.3}$$

where ϵ_{ijk} is the antisymmetric Levi-Civita tensor: $\epsilon_{ijk} = 1$ when the sequence of indices (i, j, k) is an even permutation of the sequence (1,2,3), i.e. (1,2,3), (3,1,2) and (2,3,1), while $\epsilon_{ijk} = -1$ for an odd permutation, i.e. (3,2,1), (1,3,2) and (2,1,3). If any two indices are equal, $\epsilon_{ijk} = 0$.

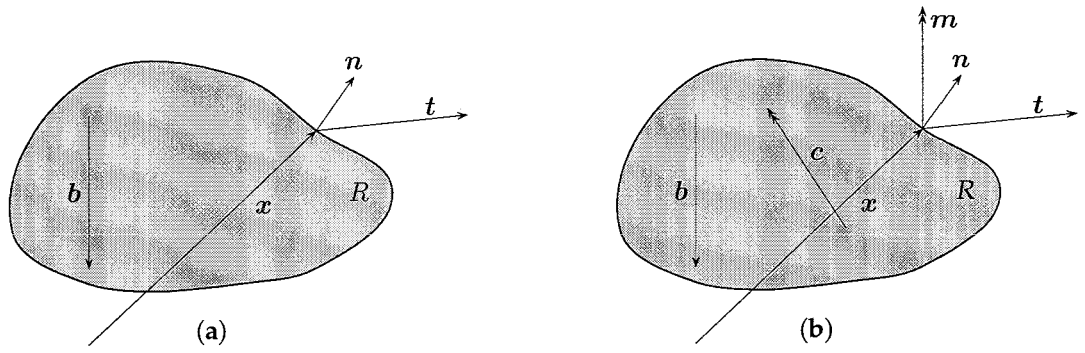

Figure 3.3: Definition of area quantities: classical (a) and Cosserat mechanics (b)

When we define $\mu_{ji} = \epsilon_{ilk} x_l \sigma_{jk}$, and use Gauß' theorem, this results in

$$\int_r \left(\frac{\partial \mu_{ji}}{\partial x_l} + \epsilon_{ijk} x_j b_k \right) \mathrm{d}\boldsymbol{x} = \mathbf{0} \quad \rightarrow \quad \frac{\partial \mu_{ji}}{\partial x_j} + \epsilon_{ijk} x_j b_k = \mathbf{0} \quad \xrightarrow{\forall r} \quad \epsilon_{ijk} \sigma_{jk} = 0 \quad \text{in } R, \tag{3.4}$$

since $\epsilon_{ijk} x_j \sigma_{lk} = \epsilon_{ilk} x_l \sigma_{jk}$. Notice that these are the classical balance laws, and that the result of the second equation is obtained by using the first balance law.

Cosserat Mechanics Approach

Here also, a material body that occupies a bounded region R is considered. The position vector is $\boldsymbol{x}$, and the displacements of a point are given by the vector $\boldsymbol{u}$, whereas the rotations are given by the vector $\boldsymbol{\varphi}$. The strain tensor will be defined as

$$\varepsilon_{ji} = \frac{\partial u_i}{\partial x_j} - \epsilon_{kji} \varphi_k \qquad \text{for } i, j = 1, 2, 3. \tag{3.5}$$

Notice that, in contrast to classical elasticity, the strain tensor is asymmetric, whilst the diagonals are the usual normal strains. Also, it can be observed that a constant rotation results in shear strains. In addition to these normal and shear strains, Cosserat theory requires the introduction of *curvatures*, which can be explained as being the 'strains' related to the difference in rotation φ_i of two points. The curvatures are defined as components of the torsion tensor

$$\kappa_{ji} = \frac{\partial \varphi_i}{\partial x_j}. \tag{3.6}$$

As will be illustrated in the next Section, the definitions for the strains and the curvatures follow naturally from the weak form of the equilibrium equations. To give an interpretation of these kinematical quantities, they are split up into a symmetric and a skew-symmetric part,

$$\varepsilon_{(ji)} = \frac{1}{2}(\varepsilon_{ji} + \varepsilon_{ij}) = \frac{1}{2}\left(\frac{\partial u_i}{\partial x_j} + \frac{\partial u_j}{\partial x_i} \right), \tag{3.7}$$

$$\varepsilon_{\langle ji \rangle} = \frac{1}{2}(\varepsilon_{ji} - \varepsilon_{ij}) = \frac{1}{2}\left(\frac{\partial u_i}{\partial x_j} - \frac{\partial u_j}{\partial x_i} \right) - \epsilon_{kji} \varphi_k. \tag{3.8}$$

Here, $(.)$ denotes the symmetric part, whereas $\langle . \rangle$ represents the skew-symmetric part of a tensor. One may conclude that the symmetric part equals the classical strain definition, whereas the skew-symmetric part includes the influence of the rotations, and the skew-symmetric part of the gradients of the displacements (i.e., the linear rotation tensor).

The external loads are represented by three vectors, a stress vector $\boldsymbol{t}$, a volume load vector $\boldsymbol{b}$, a moment vector $\boldsymbol{m}$, which is independent of $\boldsymbol{t}$, and a volume moment vector $\boldsymbol{c}$, Fig.3.3(b). For each subdomain r, the balance laws can be written as

$$\int_{\partial r} \boldsymbol{t}\,\mathrm{d}s + \int_{r} \boldsymbol{b}\,\mathrm{d}\boldsymbol{x} = \boldsymbol{0} \qquad \text{and} \qquad \int_{\partial r} (\boldsymbol{m} + \boldsymbol{x}\times\boldsymbol{t})\,\mathrm{d}s + \int_{r} (\boldsymbol{c} + \boldsymbol{x}\times\boldsymbol{b})\,\mathrm{d}\boldsymbol{x} = \boldsymbol{0}. \tag{3.9}$$

Again, using Cauchy, viz. $t_i = \sigma_{ji}n_j$, and Gauß' theorem, the force balance becomes

$$\int_{\partial r} \sigma_{ji}n_j\,\mathrm{d}s + \int_{r} b_i\,\mathrm{d}\boldsymbol{x} = 0 \quad \rightarrow \quad \int_{r} \left(\frac{\partial \sigma_{ji}}{\partial x_j} + b_i\right)\mathrm{d}\boldsymbol{x} = 0 \quad \xrightarrow{\forall r} \quad \frac{\partial \sigma_{ji}}{\partial x_j} + b_i = 0 \quad \text{in } R. \tag{3.10}$$

For the moment balance equation, we also apply Cauchy, $m_i = \mu_{ji}n_j$, where μ_{ji} is defined as the couple stress tensor (Fig.3.4), and using Gauß' divergence theorem, we get

$$\begin{aligned} &\int_{\partial r} (\mu_{ji}n_j + \epsilon_{ijk}x_j\sigma_{lk}n_l)\,\mathrm{d}s + \int_{r} (c_i + \epsilon_{ijk}x_jb_k)\,\mathrm{d}\boldsymbol{x} = \boldsymbol{0} \\ \rightarrow \quad &\int_{r} \left(\frac{\partial \mu_{ji}}{\partial x_j} + \epsilon_{ijk}\delta_{jl}\sigma_{lk} + \epsilon_{ijk}x_j\frac{\partial \sigma_{lk}}{\partial x_l} + c_i + \epsilon_{ijk}x_jb_k\right)\mathrm{d}\boldsymbol{x} = \boldsymbol{0} \\ &\xrightarrow{\forall r} \quad \frac{\partial \mu_{ji}}{\partial x_j} + \epsilon_{ijk}\sigma_{jk} + c_i = 0 \quad \text{in } R. \end{aligned} \tag{3.11}$$

The most noticable difference in the constitutive quantities, is the presence of independent moments, that is, independent of the stress tensor. These moments are inherent to the rotations as (independent) degrees of freedom. Note also that in the last equation, the volume load vector is absent as a result of using the first balance equation, and that the stress tensor now is not symmetric.

To complete the mechanical problem, constitutive equations and boundary conditions are needed. The constitutive equations can be formulated as follows, assuming isotropic, elastic material behaviour, according to Nowacki (1986),

$$\sigma_{ji} = \frac{E}{1+\nu}\left[\varepsilon_{(ji)} + \vartheta\varepsilon_{\langle ji\rangle} + \frac{\nu}{1-2\nu}\varepsilon_{kk}\delta_{ji}\right], \tag{3.12}$$

$$\mu_{ji} = \frac{D}{1+\mu}\left[\kappa_{(ji)} + \eta\kappa_{\langle ji\rangle} + \frac{\mu}{1-2\mu}\kappa_{kk}\delta_{ji}\right]. \tag{3.13}$$

where E is Young's modulus, ν Poisson's ratio, ϑ a parameter which defines the influence of the anti-symmetric part of the strains, D the equivalent of Young's modulus for the couple stresses, μ the equivalent of Poisson's ratio for the couple stresses and η similar to ϑ. Analog to the strains, the equation for the stresses can also be split up into a symmetric and anti-symmetric part to interpret them,

$$\sigma_{(ji)} = \frac{E}{1+\nu}\left[\varepsilon_{(ji)} + \frac{\nu}{1-2\nu}\varepsilon_{kk}\delta_{ji}\right], \tag{3.14}$$

$$\sigma_{\langle ji\rangle} = \frac{E}{1+\nu}\vartheta\varepsilon_{\langle ji\rangle}. \tag{3.15}$$

It is evident that the constitutive equations for the symmetric part are equal to the classical isotropic elastic case. i.e. Hooke's law. The anti-symmetric part of the constitutive equations clearly relates the anti-symmetric parts of the strains to the stresses.

The boundary Γ of the material is assumed to be divided into two disjoint parts Γ_u and Γ_t. On Γ_u, the displacements are prescribed, while on Γ_t the tractions are given. We also assume that a second partition of the boundary exists, consisting of the disjoint parts Γ_φ and Γ_m. On Γ_φ, the rotations are prescribed and on Γ_m the moments are provided. The boundary conditions on Γ now read

$$u_i = u_{0i}, \quad \text{on } \Gamma_u \qquad\qquad \sigma_{ji}n_j = t_{0i}, \quad \text{on } \Gamma_t \tag{3.16}$$

$$\varphi_i = \varphi_{0i}, \quad \text{on } \Gamma_\varphi \qquad\qquad \mu_{ji}n_j = m_{0i}, \quad \text{on } \Gamma_m \tag{3.17}$$

The Plane Strain Case

Assuming now that the deformation in one direction, x_3 say, is zero, that is, assuming that $u_3 = 0$, $\partial/\partial x_3 = 0$ and $\varphi_1 = \varphi_2 = 0$, the three-dimensional model reduces to a two-dimensional model, which is the analogon of the classic plane strain case. The strain components can be written as

$$\varepsilon_{11} = \frac{\partial u_1}{\partial x_1}, \qquad \varepsilon_{12} = \frac{\partial u_2}{\partial x_1} - \varphi_3, \tag{3.18}$$

$$\varepsilon_{21} = \frac{\partial u_1}{\partial x_2} + \varphi_3, \qquad \varepsilon_{22} = \frac{\partial u_2}{\partial x_2}. \tag{3.19}$$

For convenience, the index 3 in φ will be omitted. The curvature components read

$$\kappa_{13} = \frac{\partial \varphi}{\partial x_1} \quad \text{and} \quad \kappa_{23} = \frac{\partial \varphi}{\partial x_2}. \tag{3.20}$$

Finally, the equilibrium equitions can be written as

$$\frac{\partial \sigma_{11}}{\partial x_1} + \frac{\partial \sigma_{21}}{\partial x_2} = 0, \tag{3.21}$$

$$\frac{\partial \sigma_{12}}{\partial x_1} + \frac{\partial \sigma_{22}}{\partial x_2} = 0, \tag{3.22}$$

$$\frac{\partial \mu_{13}}{\partial x_1} + \frac{\partial \mu_{23}}{\partial x_2} + (\sigma_{12} - \sigma_{21}) = 0. \tag{3.23}$$

A graphical representation of the stress components and the couple stresses is given in Fig.3.4.

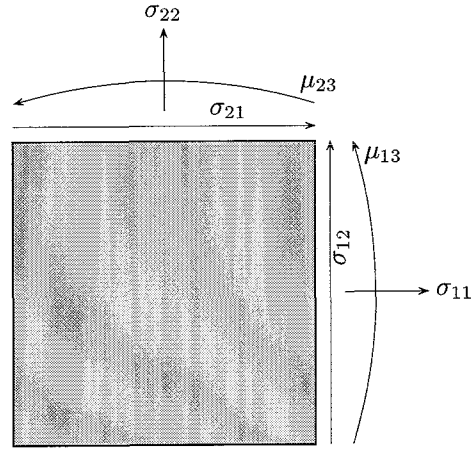

Figure 3.4: Definition of kinematical quantities of a Cosserat medium

We define the following quantities,

$$\underset{\sim}{\varepsilon} = \left(\varepsilon_{11}\ \varepsilon_{22}\ \varepsilon_{12}\ \varepsilon_{21}\ \kappa_{13}\ \kappa_{23}\right)^T, \quad \underset{\sim}{\sigma} = \left(\sigma_{11}\ \sigma_{22}\ \sigma_{12}\ \sigma_{21}\ \mu_{13}\ \mu_{23}\right)^T, \quad \underline{u} = \left(u_1\ u_2\ \varphi\right)^T. \tag{3.24}$$

Using this, the constitutive equations (3.12) and (3.13), can be written in matrix form,

$$\begin{pmatrix}\sigma_{11}\\ \sigma_{22}\\ \sigma_{12}\\ \sigma_{21}\\ \mu_{13}\\ \mu_{23}\end{pmatrix} = \frac{E}{1+\nu}\begin{pmatrix} \frac{1-\nu}{1-2\nu} & \frac{\nu}{1-2\nu} & 0 & 0 & 0 & 0\\ \frac{\nu}{1-2\nu} & \frac{1-\nu}{1-2\nu} & 0 & 0 & 0 & 0\\ 0 & 0 & \frac{1+\vartheta}{2} & \frac{1-\vartheta}{2} & 0 & 0\\ 0 & 0 & \frac{1-\vartheta}{2} & \frac{1+\vartheta}{2} & 0 & 0\\ 0 & 0 & 0 & 0 & \frac{DP}{E}(1+\nu) & 0\\ 0 & 0 & 0 & 0 & 0 & \frac{DP}{E}(1+\nu) \end{pmatrix}\begin{pmatrix}\varepsilon_{11}\\ \varepsilon_{22}\\ \varepsilon_{12}\\ \varepsilon_{21}\\ \kappa_{13}\\ \kappa_{23}\end{pmatrix}, \tag{3.25}$$

where we define the constant $P = (1+\eta)/2(1+\mu)$. Note that in the stress and strain columns, both the translational as well as the rotational components are included, clearly to arrive at one stiffness matrix. Note also that by choosing the plane strain conditions, μ_{31} is dependent on μ_{13} and subsequently, μ_{32} is dependent on μ_{23}. This can be recognized as the likewise dependency which, in the plane strain case, exists between σ_{33} on one hand, and σ_{11} and σ_{22} on the other hand.

3.2 Weak Form of the Equilibrium Equations

The basis of the finite element method is formed by the *weak formulation* of the problem, that is obtained by multiplying the equilibrium equations with weighting functions and integrating over the domain Ω. In the sequel, we will neglect the volume forces and volume moments, which results in the following integral equation

$$\int_\Omega \left[v_i \frac{\partial \sigma_{ji}}{\partial x_j} + \psi_i \left(\epsilon_{ijk}\sigma_{jk} + \frac{\partial \mu_{ji}}{\partial x_j} \right) \right] \mathrm{d}\Omega = 0 \qquad \forall v_i,\ \psi_i, \tag{3.26}$$

where v_i and ψ_i are weighting functions. Integrating by parts yields

$$\int_\Omega \left[\left(\frac{\partial v_i}{\partial x_j} - \psi_k \epsilon_{kji} \right)\sigma_{ji} + \frac{\partial \psi_i}{\partial x_j}\mu_{ji} \right] \mathrm{d}\Omega = \int_\Gamma \left[v_i\, t_i + \psi_i\, m_i \right] \mathrm{d}\Gamma \qquad \forall v_i,\ \psi_i. \tag{3.27}$$

It is important to notice that the term between brackets in front of σ_{ji} can be identified with the definition of the strains, (3.5). The term in front of μ_{ji} is analogous to the definition of the curvatures, (3.6). So, the definitions of the strain and curvature components follow in a natural way from the weak form of the equilibrium equations.

For the two-dimensional plane strain case, we define a matrix with differential operators (see also Appendix C),

$$\underline{L} = \begin{pmatrix} \frac{\partial}{\partial x_1} & 0 & 0 & \frac{\partial}{\partial x_2} & 0 & 0\\ 0 & \frac{\partial}{\partial x_2} & \frac{\partial}{\partial x_1} & 0 & 0 & 0\\ 0 & 0 & -1 & 1 & \frac{\partial}{\partial x_1} & \frac{\partial}{\partial x_2} \end{pmatrix}^T. \tag{3.28}$$

With this definition, it follows that $\underset{\sim}{\varepsilon} = \underline{L}\,\underset{\sim}{u}$ and $\underset{\sim}{\sigma} = \underline{S}(\underset{\sim}{\varepsilon})$, the latter representing the constitutive equations. Using (3.24) and (3.28) accompanied with the definitions $\underset{\sim}{w} = (v_1\, v_2\, \psi_3)^T$ and $\underset{\sim}{t} = (t_1\, t_2\, m_3)^T$, we obtain the weak form in matrix notation

$$\int_\Omega (\underline{L}\underset{\sim}{w})^T \underline{S}\,(\underline{L}\underset{\sim}{u})\ \mathrm{d}\Omega = \int_\Gamma \underset{\sim}{w}^T \underset{\sim}{t}\ \mathrm{d}\Gamma. \tag{3.29}$$

In general, (3.29) is a non-linear relation for the displacement field $\underset{\sim}{u}$, so we have to use an iterative procedure to solve it. Using a standard Newton-Rhapson iteration procedure, we decompose $\underset{\sim}{u}$ in $\underset{\sim}{u}^* + \delta\underset{\sim}{u}$, where $\underset{\sim}{u}^*$ is the displacement estimation and $\delta\underset{\sim}{u}$ the correction of this estimation. Linearising the constitutive equation, with respect to $\delta\underset{\sim}{u}$,

$$\underline{S}\,(\underline{L}\,\underset{\sim}{u}) = \underline{S}\,(\underline{L}\,\underset{\sim}{u}^*) + \frac{\partial \underline{S}}{\partial \underset{\sim}{\varepsilon}}\underline{L}\,\delta\underset{\sim}{u}, \tag{3.30}$$

yields the linearised weak, iterative formulation of the equilibrium equations

$$\int_\Omega (\underline{L}\underset{\sim}{w})^T \frac{\partial \underline{S}}{\partial \underset{\sim}{\varepsilon}}\underline{L}\,\delta\underset{\sim}{u}\,\mathrm{d}\Omega = \int_\Gamma \underset{\sim}{w}^T \underset{\sim}{t}\,\mathrm{d}\Gamma - \int_\Omega (\underline{L}\underset{\sim}{w})^T \underset{\sim}{\sigma}^*\,\mathrm{d}\Omega. \tag{3.31}$$

where $\underset{\sim}{\sigma}^*$ represents the estimation of the stress, as a result of the estimation of the displacement field, acoording to $\underset{\sim}{\sigma}^* = \underline{S}\,(\underline{L}\,\underset{\sim}{u}^*)$.

3.3 Finite Element Discretization

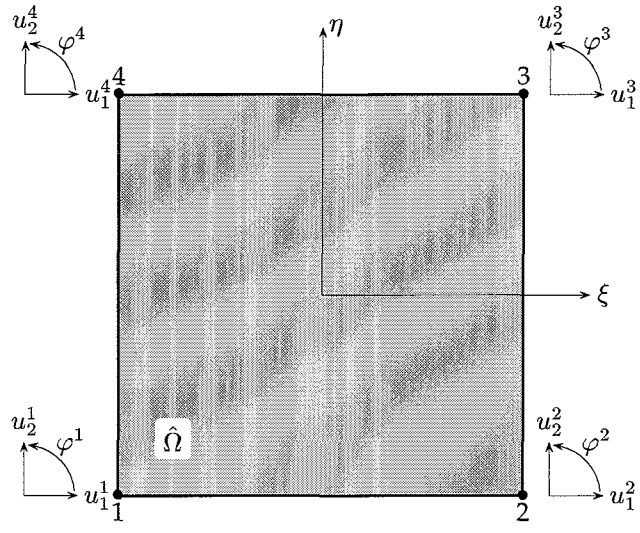

Figure 3.5: 4 Noded isoparametric element with three degrees of freedom at each node

In this Section, we will formulate the discretized equilibrium equations for a four noded quadrilateral, isoparametric Cosserat element, with 3 degrees of freedom at each node, being two displacements and one rotation (Fig. 3.5).

Now, when defining a new element, the element stiffness matrix and the right hand side must be formulated, following from the weak form of the equilibrium equations. The discretized form of (3.31) can be written as follows, when the total domain Ω is subdivided into e elements with area Ω^e,

$$\sum_e \int_{\Omega^e} (\underline{L}\underset{\sim}{w})^T \frac{\partial \underline{S}}{\partial \underset{\sim}{\varepsilon}}\underline{L}\,\delta\underset{\sim}{u}\,\mathrm{d}\Omega^e = \sum_e \int_{\Gamma^e} \underset{\sim}{w}^T \underset{\sim}{t}\,\mathrm{d}\Gamma^e - \sum_e \int_{\Omega^e} (\underline{L}\underset{\sim}{w})^T \underset{\sim}{\sigma}^*\,\mathrm{d}\Omega^e. \tag{3.32}$$

This equation will now be interpolated, making use of an isoparametric formulation and Galerkin's method, see e.g. Zienkiewicz (1977) and Baaijens (1994).

The term isoparametric indicates that the same shape functions (interpolation functions) are used to define the element's geometric shape as are used to define the displacements within the element.

The element contributions are formulated using a *natural coordinate system* (ξ, η) that is defined by the element geometry and not by the element orientation in the global coordinate system. A relation (*transformation mapping*) exists between the natural coordinate system and the global coordinate system for each element of a specific structure.

Following Logan (1992), we can write the natural (local) coordinates

$$x(\xi,\eta) = \sum_{a=1}^{n_{nd}} N_a(\xi,\eta)\, x_a, \tag{3.33}$$

$$y(\xi,\eta) = \sum_{a=1}^{n_{nd}} N_a(\xi,\eta)\, y_a. \tag{3.34}$$

In these equations, n_{nd} is the number of nodes per element, N_a is defined as the shape function for each node a, whereas (x_a, y_a) are the node coordinates. Hence, we can establish expressions for the individual shape functions,

$$\begin{aligned} N_1 &= \frac{1}{4}(1-\xi)(1-\eta), \qquad & N_2 &= \frac{1}{4}(1+\xi)(1-\eta), \\ N_3 &= \frac{1}{4}(1+\xi)(1+\eta), \qquad & N_4 &= \frac{1}{4}(1-\xi)(1+\eta). \end{aligned} \tag{3.35}$$

Thus, this bilinear relation maps the (ξ, η) coordinates of any point in the element to the global (x, y) coordinates. For other element classes, shape functions can be found in Zienkiewicz (1977).

The definition of an isoparametric element enables us to interpolate the displacements and rotation using the same shape functions N_a,

$$\underset{\sim}{u}(\xi,\eta) = \underline{N}^T(\xi,\eta)\, \underset{\sim}{u}^e \tag{3.36}$$

where $\underset{\sim}{u}^e$ contains the nodal values of the degrees of freedom, and $\underline{N}^T$ the matrix with the nodal values of the shape functions,

$$\underline{N}^T = \begin{pmatrix} N_1 & 0 & 0 & N_2 & 0 & 0 & N_3 & 0 & 0 & N_4 & 0 & 0 \\ 0 & N_1 & 0 & 0 & N_2 & 0 & 0 & N_3 & 0 & 0 & N_4 & 0 \\ 0 & 0 & N_1 & 0 & 0 & N_2 & 0 & 0 & N_3 & 0 & 0 & N_4 \end{pmatrix} \tag{3.37}$$

Adopting Galerkin's method, which states that the interpolation functions used with the displacements and the weighting functions may be chosen equally,

$$\underset{\sim}{w}(\xi,\eta) = \underline{N}^T(\xi,\eta)\, \underset{\sim}{w}^e, \tag{3.38}$$

with $\underset{\sim}{w} = (v_1\, v_2\, \psi_3)^T$ a column of test functions, and $\underset{\sim}{w}^e$ a column containing the values of the test functions at the nodes.

Writing $\underset{\sim}{\varepsilon}(\underset{\sim}{u}) = \underline{B}\, \underset{\sim}{u}^e$ (see Appendix C for the expression of the $\underline{B}$ matrix), we are able to rewrite (3.32) as

$$\sum_e (\underset{\sim}{w}^e)^T \int_{\Omega^e} (\underline{B})^T \frac{\partial \underset{\sim}{S}}{\partial \underset{\sim}{\varepsilon}} \underline{B}\, \mathrm{d}\Omega^e\, \delta \underset{\sim}{u}^e = \sum_e (\underset{\sim}{w}^e)^T \int_{\Gamma^e} \underline{N}\, \underset{\sim}{t}\, \mathrm{d}\Gamma^e - \sum_e (\underset{\sim}{w}^e)^T \int_{\Omega^e} (\underline{B})^T \underset{\sim}{\sigma}^*\, \mathrm{d}\Omega^e. \tag{3.39}$$

We now define the element stiffness matrix

$$\underline{K}^e = \int_{\Omega^e} (\underline{B})^T \frac{\partial \underset{\sim}{S}}{\partial \underset{\sim}{\varepsilon}} \underline{B}\, \mathrm{d}\Omega^e. \tag{3.40}$$

The resulting matrix has the dimensions 12×12, which can be subdivided in 16 submatrices, $\underline{K}^e_{ij}$, with dimensions 3×3,

$$\underline{K}^e = \begin{pmatrix} \underline{K}^e_{11} & \cdots & \underline{K}^e_{14} \\ \vdots & & \vdots \\ \underline{K}^e_{41} & \cdots & \underline{K}^e_{44} \end{pmatrix}. \tag{3.41}$$

The intended 3×3 submatrices $\underline{K}^e_{ij}$ reads,

$$\underline{K}^e_{ij} = \int_{\Omega^e} \begin{pmatrix} k_{11} & k_{12} & k_{13} \\ k_{21} & k_{22} & k_{23} \\ k_{31} & k_{32} & k_{33} \end{pmatrix} \mathrm{d}\Omega^e. \tag{3.42}$$

The right hand side in matrix form can be written as

$$\underset{\sim}{r}^e = \int_{\Gamma^e} \underline{N}\,\underset{\sim}{t}\,\mathrm{d}\Gamma^e - \int_{\Omega^e} (\underline{B})^T \underset{\sim}{\sigma}^*\,\mathrm{d}\Omega^e. \tag{3.43}$$

The characteristic finite element equations to be solved, may now be formulated as

$$\underline{K}^e\,\delta\underline{u}^e = \underset{\sim}{r}^e \tag{3.44}$$

To check these results, the element has been implemented in the programming environment Matlab and some tests have been performed.

3.4 Element Validation

The verification of the element is essential and will be shown here. The used constitutive equations are given by (3.25).

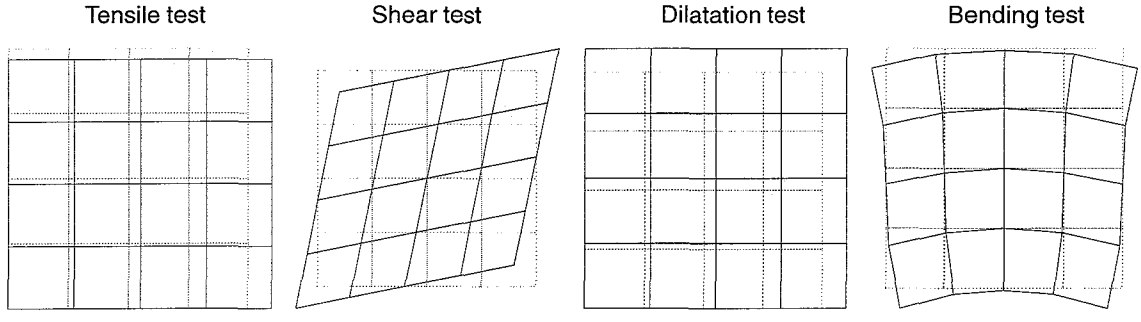

Figure 3.6: Test configurations: dotted lines=undeformed; solid lines=deformed

The Cosserat element has been subjected to some test problems (Fig. 3.6): a tensile test, a shear test, a dilatation test and a bending test. These tests are compared with analytical solutions. The relevant deformation measures (stresses and strains) can be found in Table 3.1. We may conclude from these values, that the element is implemented correctly.

Anticipating the strain softening behaviour resulting from our homogenization process described in the next Chapter and in Vosbeek (1994), we will define a function for the E-modulus of the macroscopic medium. This function is given in terms of a, yet to be determined, equivalent strain measure. In principle, the above described element does not suffer from mesh dependency (De Borst 1990), and can be used to simulate localization of deformation, or, more generally, strain softening behaviour.

3.5 Strain Softening using Cosserat Mechanics

In this Section, first we assume an E-modulus as a function of an equivalent strain measure. Next, we show results of some 'benchmark' problems and the effect of mesh-size.

TEST		MATLAB	ANALYTICAL
tensile	ε_{11}	0.1	0.1
	ε_{22}	-0.0429	-0.0429
	σ_{11}	0.1099	0.1099
shear	ε_{12}	0.2	0.2
	ε_{21}	0.2	0.2
	σ_{12}	0.154	0.154
	σ_{21}	0.154	0.154
dilatation	ε_{11}	0.1	0.1
	ε_{22}	0.1	0.1
	σ_{11}	0.192	0.192
	σ_{22}	0.192	0.192
bending	κ_{13}	-0.1	-0.1
	μ_{13}	-0.2	-0.2

Table 3.1: The test results

3.5.1 The Definition of the E-modulus

The definition of the E-modulus as function of the equivalent strain, Fig.3.7, is given by

$$\begin{aligned} E(\varepsilon_{eq}) &= E_0 && 0 < \varepsilon_{eq} < \varepsilon_0, \\ E(\varepsilon_{eq}) &= E_0\left[(1+\zeta)\frac{\varepsilon_0}{\varepsilon_{eq}} - \zeta\right] && \varepsilon_0 \leq \varepsilon_{eq} < \varepsilon_1, \\ E(\varepsilon_{eq}) &= E_0\left[(1+\zeta)\frac{\varepsilon_0}{\varepsilon_{eq}} - (\zeta+\chi)\frac{\varepsilon_1}{\varepsilon_{eq}} + \chi\right] && \varepsilon_{eq} \geq \varepsilon_1. \end{aligned} \tag{3.45}$$

Here, E_0 is the initial (elastic) modulus, ε_0 is the strain at which softening occurs, ζ is the slope of the softening branch, ε_1 is the strain at which hardening occurs, and χ is the slope of the hardening branch.

3.5.2 Implementation of the E-modulus

Again, the constitutive equations are given by (3.12) and (3.13). From dimension analysis, it follows that the ratio of D and E has the dimension $[m^2]$. The obvious choice then is to relate E and D by introducing a length scale parameter ℓ,

$$D(\varepsilon_{eq}) = E(\varepsilon_{eq})\,\ell^2. \tag{3.46}$$

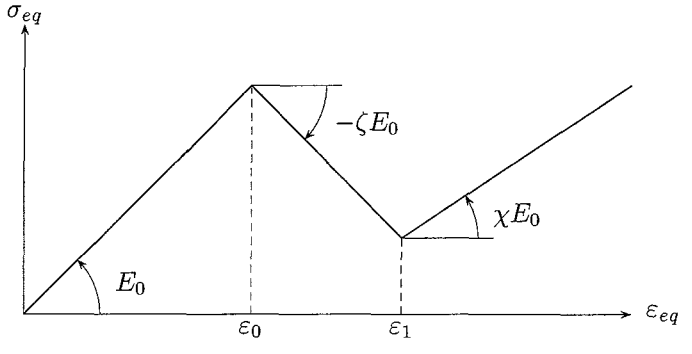

Figure 3.7: The equivalent stress versus equivalent strain for the given definition of the E-modulus

The relation between the stresses and strains can then be written as

$$\hat{\sigma}_i = \frac{E(\varepsilon_{eq})}{1+\nu} C_{ik}\, \hat{\varepsilon}_k \qquad \text{for } i,k = 1,\ldots,6, \tag{3.47}$$

where C_{ij} is the matrix

$$\underline{C} = \begin{bmatrix} \frac{1-\nu}{1-2\nu} & \frac{\nu}{1-2\nu} & 0 & 0 & 0 & 0 \\ \frac{\nu}{1-2\nu} & \frac{1-\nu}{1-2\nu} & 0 & 0 & 0 & 0 \\ 0 & 0 & \frac{1+\vartheta}{2} & \frac{1-\vartheta}{2} & 0 & 0 \\ 0 & 0 & \frac{1-\vartheta}{2} & \frac{1+\vartheta}{2} & 0 & 0 \\ 0 & 0 & 0 & 0 & \ell^2 P(1+\nu) & 0 \\ 0 & 0 & 0 & 0 & 0 & \ell^2 P(1+\nu) \end{bmatrix}, \tag{3.48}$$

and $\hat{\sigma}_i$ and $\hat{\varepsilon}_k$ according to the i-th and k-th component of the columns defined in (3.24), respectively. The derivatives of $\hat{\sigma}_i$ with respect to $\hat{\varepsilon}_k$ are needed to formulate the element stiffness matrix,

$$\frac{\partial \hat{\sigma}_i}{\partial \hat{\varepsilon}_j} = \frac{E}{1+\nu} C_{ij} + \frac{1}{1+\nu} C_{ik}\hat{\varepsilon}_k \frac{\partial E}{\partial \varepsilon_{eq}} \frac{\partial \varepsilon_{eq}}{\partial \hat{\varepsilon}_j} \qquad \text{for } i,j,k = 1,\ldots,6. \tag{3.49}$$

To calculate $\partial\varepsilon_{eq}/\partial\varepsilon_j$, we need a definition of the equivalent strain. De Borst (1990) proposed $\varepsilon_{eq} = \sqrt{3J}$ in which J, for a micro-polar continuum, is given by

$$J = \frac{1}{4}\varepsilon^d_{ij}\varepsilon^d_{ij} + \frac{1}{4}\varepsilon^d_{ji}\varepsilon^d_{ji} + \frac{1}{2}\ell^2\kappa_{ij}\kappa_{ij}. \tag{3.50}$$

where the superscript d represents the deviatoric part of a tensor. For the two-dimensional plane strain case, we then have

$$\varepsilon_{eq} = \sqrt{\varepsilon^2_{11} + \varepsilon^2_{22} - \varepsilon_{11}\varepsilon_{22} + \frac{3}{4}(\varepsilon_{12}+\varepsilon_{21})^2 + \frac{3}{2}\ell^2(\kappa^2_{13}+\kappa^2_{23})}. \tag{3.51}$$

The derivatives of ε_{eq} with respect to ε_j are given in Appendix C. In the next Section, some results are shown.

3.6 Strain Softening Results

Some benchmark problems will be shown in this Section, to prove the capability of the element to describe strain softening, and to show the mesh-size dependency. First a tensile test will be executed, Fig.3.8(a). The displacements will be prescribed, and at the upper left corner, an imperfection in the cross-section will be used to initiate a stress concentration. This will result in a localization zone. After that, a shear test is simulated, Fig.3.8(b). Here, a displacement will be prescribed at the upper right corner of the specimen. An imperfection is not needed to trigger localization.

3.6.1 Tensile Test

The first benchmark problem is an tensile test. A geometric imperfection, with a value of 1% of the original cross-section, is used to trigger localization at the upper left corner of the test specimen. Symmetry is assumed, so the boundary conditions depicted in Fig.3.8(a) may be applied. At the edges of symmetry, in addition, the rotations will be suppressed, also in view of symmetry. In Fig.3.9, some deformation stages are shown as well as the resulting force-displacement curve. This shows the capability of the element to describe strain softening. The used material parameters are: $E_0 = 100$ [MPa], $\nu = 0.3, \zeta = 0.02, \chi = 0.04, \varepsilon_0 = 0.005, \varepsilon_1 = 0.03, \vartheta = 0.8, P = 0.5$, and $\ell = 0.1$ [m].

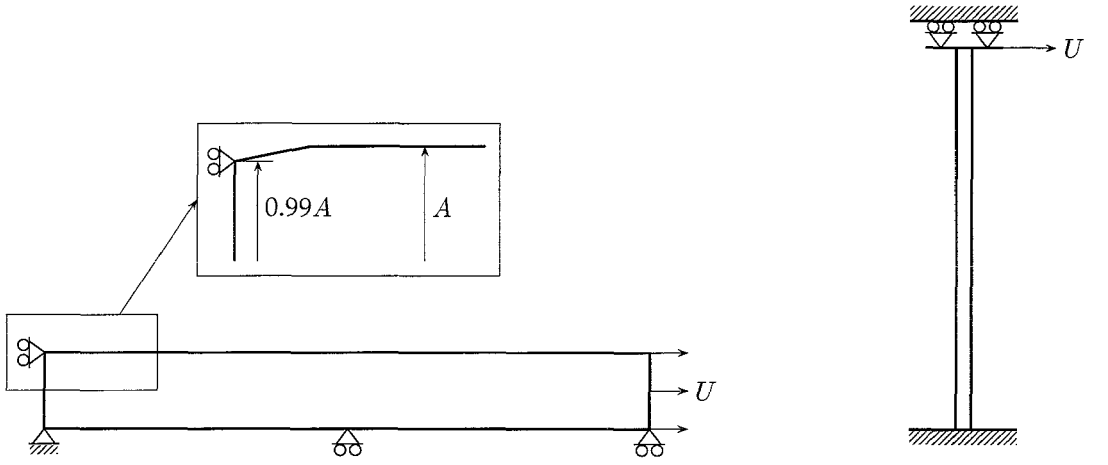

(a) (b)

Figure 3.8: The test configurations: (a) tensile test and (b) shear test

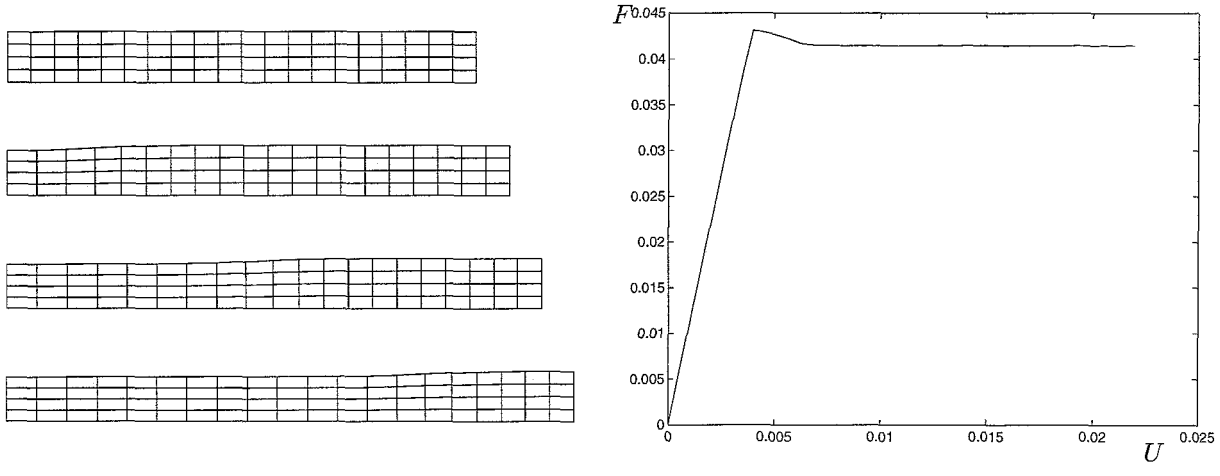

Figure 3.9: Deformation stages of the tensile specimen and the resulting load-displacement curve

3.6.2 Shear Test

The next problem is an infinitely long shear layer. The bottom of the shear layer is fixed ($u_1 = u_2 = 0$) and the upper boundary is subjected to a horizontal displacement U, Fig.3.8(b). The condition $\varphi = 0$ has been enforced at the upper and lower boundaries. Conventional continua show snap-back behaviour upon mesh refinement and a localization zone which is dependent of the element size (De Borst 1990). Using a Cosserat element, an imperfection is not necessary to trigger localization, since the boundary conditions result in a non-homogeneous strain distribution. Fig.3.10 shows some deformation stages of three different discretizations of the problem, i.e., a finite element mesh of 20, 40 and 80 elements, respectively. In Fig.3.11, the resulting load displacement curves are depicted. From these results, it is obvious that the solution is mesh-independent, as was expected.

It should be noticed that the initiation of the localization is influenced by the choice of the material parameters. For some specific values, localization did not occur at all. A reason for this may be that the number of degrees of freedom of the material is not quite enough in these situations. In the next Chapter, we will determine the parameters of the E-modulus by a homogenization procedure. The obtained constitutive equations will be used on some finite element calculations.

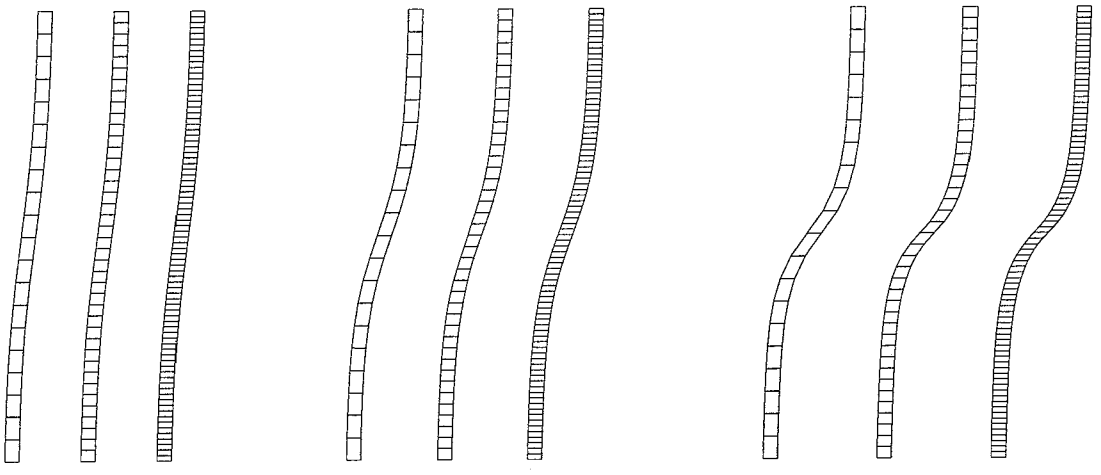

Figure 3.10: Deformation stages of the shear test for the different finite element meshes of 20, 40 and 80 elements

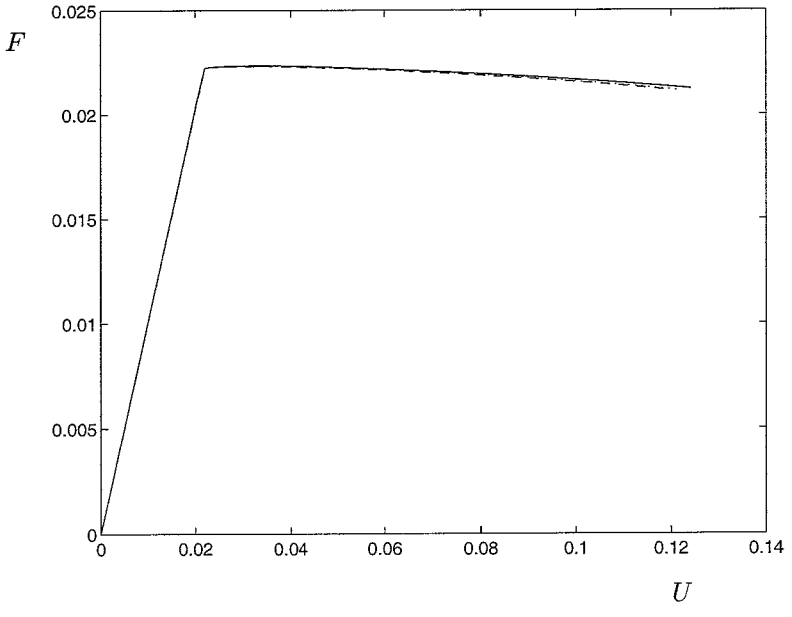

Figure 3.11: The load-displacement curve for the different meshes. 20 elements (solid), 40 elements (dotted) and 80 element (dashed)

4 Homogenization towards Cosserat Media

In the introductory Chapter, it was argued that the model material is not statistically homogeneous since this material exhibits localization of deformation. Hence, homogenization methods must be used which result in non-local models. In Chapter 2, homogenization theory was discussed. A non-local constitutive equation was derived using derivatives of the macroscopic strain as additional quantities. The physical interpretation of these quantities is not clear. Cosserat theory provides additional quantities in terms of rotational degrees of freedom. In the preceding Chapter, this theory was elucidated. As was seen in the Introduction, the first step of the homogenization process is the definition of the relation between the macroscopic and microscopic state variables. Since the macroscopic deformation variables will be prescribed on the boundary on the RVE using these definitions, the relation between the macroscopic deformation and constitutive quantities can be obtained.

In this Chapter, we first derive microscopic boundary conditions which may be applied to a representative volume element. The boundary conditions will be formulated in terms of displacements, which are parameterized by the macroscopic deformation quantities. These quantities are identified by the Cosserat theory. Next, we apply these boundary conditions to get the averaged microscopic constitutive quantities. The obtained curves of these quantities then will be fitted onto the chosen function of the E-modulus, given in the preceding Chapter. Some finite element calculations will be performed using these parameters.

4.1 Displacement Field I

Let $\boldsymbol{x}$ be the position of a material point of the macroscopic continuum, and let $\boldsymbol{y}$ be the position of a material point in the RVE associated with the material point $\boldsymbol{x}$. In the sequel, the symbols with an overstrike character represent the macroscopic quantities, and the symbols without these overstrike characters are the microscopic quantities. Let us now split up the microscopic displacement field into a rigid body motion and a part representing the actual deformation,

$$\boldsymbol{u}(\boldsymbol{x},\boldsymbol{y}) = \bar{\boldsymbol{u}}_0 + \bar{\boldsymbol{\varphi}} \times \boldsymbol{y} + \boldsymbol{v}(\boldsymbol{x},\boldsymbol{y}), \qquad \boldsymbol{v}(\boldsymbol{x},\boldsymbol{0}) = \boldsymbol{0}, \tag{4.1}$$

where the first two terms represent the rigid macroscopic motion (rigid translation and rigid rotation) and the last term symbolises the (true) deformation which ultimatively causes stresses and strains in the material.

This form of $\boldsymbol{u}$ can be written out in two dimensions

$$\begin{pmatrix} u_1 \\ u_2 \end{pmatrix} = \begin{pmatrix} \bar{u}_{01} - \bar{\varphi}_3 y_2 + v_1 \\ \bar{u}_{02} + \bar{\varphi}_3 y_1 + v_2 \end{pmatrix}. \tag{4.2}$$

Now, some relations between the microscopic and macroscopic deformation quantities have to be defined.

4.1.1 The Relation between Microscopic and Macroscopic Quantities

Since the first step of the homogenization process is defining the relation between the macroscopic and microscopic quantities, we define the macroscopic gradient of the displacement field as the average of the gradient of the microscopic displacement field,

$$\frac{\partial \bar{u}_i}{\partial x_j} = \left\langle \frac{\partial u_i}{\partial y_j} \right\rangle. \tag{4.3}$$

With (3.5) and (4.2), we then have

$$\bar{\varepsilon}_{ji} = \left\langle \frac{\partial v_i}{\partial y_j} \right\rangle. \tag{4.4}$$

Thus, we have established a relation between the microscopic deformation field $\boldsymbol{v}$ and the macroscopic deformation quantities $\bar{\varepsilon}$. Continuing this strategy, we now have to define relations between the macroscopic curvatures $\bar{\kappa}$ and the microscopic quantities. For this purpose, we define the local rotation tensor to be the anti-symmetric part of the gradient of the displacement field,

$$\omega_{ij} = \frac{1}{2}\left(\frac{\partial u_i}{\partial y_j} - \frac{\partial u_j}{\partial y_i}\right). \tag{4.5}$$

For example, the (2,1)-component of this tensor is equal to

$$\omega_{21} = \frac{1}{2}\left(\frac{\partial u_2}{\partial y_1} - \frac{\partial u_1}{\partial y_2}\right) = \frac{1}{2}\left(\frac{\partial v_2}{\partial y_1} - \frac{\partial v_1}{\partial y_2}\right) + \bar{\varphi}_3 \stackrel{\text{def}}{=} \omega^*_{21} + \bar{\varphi}_3. \tag{4.6}$$

Note that ω_{21}, which in fact is the total rotation of the material point at position $\boldsymbol{y}$ around the origin, now is split up into a rigid rotation, $\bar{\varphi}_3$, and a rotation ω^*_{21} caused by the true deformation $\boldsymbol{v}$. Since $\bar{\varphi}_3$ is constant, we define the microscopic curvatures as the gradients of rotation component ω_{21},

$$\kappa_{13} = \frac{\partial \omega_{21}}{\partial y_1} \qquad \text{and} \qquad \kappa_{23} = \frac{\partial \omega_{21}}{\partial y_2}. \tag{4.7}$$

Finally, we may define the micro-macro relations of the curvatures

$$\bar{\kappa}_{13} = \langle \kappa_{13} \rangle = \left\langle \frac{\partial \omega_{21}}{\partial y_1} \right\rangle \qquad \text{and} \qquad \bar{\kappa}_{23} = \langle \kappa_{23} \rangle = \left\langle \frac{\partial \omega_{21}}{\partial y_2} \right\rangle. \tag{4.8}$$

Next, these definitions can be used to obtain the constitutive equations by applying boundary conditions, in terms of the macroscopic deformation quantities, to the RVE.

4.1.2 The Displacement Field

To obtain an expression for $\boldsymbol{v}$, we follow the same strategy as in Chapter 2. We expand $\boldsymbol{v}$ into a Taylor series around the origin of the RVE, $\boldsymbol{y} = \boldsymbol{0}$, disregarding terms of order $\mathcal{O}(\|\boldsymbol{y}\|^3)$, and keeping $\boldsymbol{x}$ constant,

$$v_i(\boldsymbol{x},\boldsymbol{y}) = v_{0i}(\boldsymbol{x}) + \frac{\partial v_i(\boldsymbol{x},\boldsymbol{y})}{\partial y_j}\bigg|_{\boldsymbol{y}=\boldsymbol{0}} y_j + \frac{1}{2}\frac{\partial^2 v_i(\boldsymbol{x},\boldsymbol{y})}{\partial y_j \partial y_k}\bigg|_{\boldsymbol{y}=\boldsymbol{0}} y_j y_k = \alpha_{ij} y_j + \frac{1}{2}\beta_{ijk} y_j y_k, \tag{4.9}$$

where, according to (4.1), we have $v_{0i}(\boldsymbol{x}) = 0$. Taking the first and second order gradients of this expression, and averaging these expressions over the RVE volume V, yields

$$\left\langle \frac{\partial v_i}{\partial y_j} \right\rangle = \alpha_{ij} + \beta_{ijk} M^{(1)}_k, \tag{4.10}$$

$$\left\langle \frac{\partial^2 v_i}{\partial y_j \partial y_k} \right\rangle = \beta_{ijk}, \tag{4.11}$$

where $M^{(1)}_i$ is a geometry parameter, as discussed in Chapter 2. Taking a square RVE, i.e. $y_1, y_2 \in [-a, a]$, thus $M^{(1)}_i = 0$, results with (4.4) in the equality $\alpha_{ij} = \bar{\varepsilon}_{ji}$. Using (4.8), we have

$$\bar{\kappa}_{13} = \frac{\partial \omega_{21}}{\partial y_1} \stackrel{(4.6)}{=} \frac{1}{2}\left(\frac{\partial^2 u_2}{\partial y_1^2} - \frac{\partial^2 u_1}{\partial y_1 \partial y_2}\right) = \frac{1}{2}\left(\frac{\partial^2 v_2}{\partial y_1^2} - \frac{\partial^2 v_1}{\partial y_1 \partial y_2}\right) = \frac{1}{2}(\beta_{211} - \beta_{112}), \tag{4.12}$$

$$\bar{\kappa}_{23} = \frac{\partial \omega_{21}}{\partial y_2} \stackrel{(4.6)}{=} \frac{1}{2}\left(\frac{\partial^2 u_2}{\partial y_1 \partial y_2} - \frac{\partial^2 u_1}{\partial y_2^2}\right) = \frac{1}{2}\left(\frac{\partial^2 v_2}{\partial y_1 \partial y_2} - \frac{\partial^2 v_1}{\partial y_2^2}\right) = \frac{1}{2}(\beta_{212} - \beta_{122}). \tag{4.13}$$

Finally, we have obtained the formulation of the displacement field in terms of macroscopic deformation quantities,

$$u_1 = u_{01} - \bar{\varphi}_3 y_2 + \bar{\varepsilon}_{11} y_1 + \bar{\varepsilon}_{21} y_2 \qquad -\bar{\kappa}_{13} y_1 y_2 - \frac{1}{2}\bar{\kappa}_{23} y_2^2, \tag{4.14}$$

$$u_2 = u_{02} + \bar{\varphi}_3 y_1 + \bar{\varepsilon}_{12} y_1 + \bar{\varepsilon}_{22} y_2 + \frac{1}{2}\bar{\kappa}_{13} y_1^2 + \bar{\kappa}_{23} y_1 y_2. \tag{4.15}$$

To validate this displacement field, we define the macroscopic potential energy $\bar{\Psi} = \bar{\Psi}(\bar{\varepsilon}_{ji}, \bar{\kappa}_{ji})$ as the volume average of its microscopic equivalent $\Psi = \Psi(\varepsilon_{ji})$,

$$\bar{\Psi}(\bar{\varepsilon}_{ji}, \bar{\kappa}_{ji}) = \frac{1}{V} \int_R \Psi(\varepsilon_{ji}) \, \mathrm{d}\boldsymbol{y}. \tag{4.16}$$

Then, the macroscopic stress and the macroscopic couple stress are, by definition,

$$\bar{\sigma}_{ji} = \frac{\partial \bar{\Psi}}{\partial \bar{\varepsilon}_{ji}} = \frac{1}{V} \int_R \frac{\partial \Psi}{\partial \bar{\varepsilon}_{ji}} \, \mathrm{d}\boldsymbol{y} = \frac{1}{V} \int_R \sigma_{lk} \frac{\partial \varepsilon_{lk}}{\partial \bar{\varepsilon}_{ji}} \, \mathrm{d}\boldsymbol{y}, \tag{4.17}$$

$$\bar{\mu}_{ji} = \frac{\partial \bar{\Psi}}{\partial \bar{\kappa}_{ji}} = \frac{1}{V} \int_R \sigma_{lk} \frac{\partial \varepsilon_{lk}}{\partial \bar{\kappa}_{ji}} \, \mathrm{d}\boldsymbol{y}. \tag{4.18}$$

When ε_{ji} is the local strain according to the displacement field of (4.14) and (4.15), then $\partial \varepsilon_{ji} / \partial \bar{\varepsilon}_{kl} = \boldsymbol{I}$. Because the local stress σ_{ji} is symmetric, the macroscopic stress will also be symmetric, which is in conflict with Cosserat theory. Hence, the boundary conditions, (4.14) and (4.15) are not in concurrence with the imposed requirements. In the next Section, we will derive a displacement field, which is consistent with the definitions concerning the relation between macroscopic and microscopic variables. The difference in approach lies in the splitting up of the variables in symmetric and skew-symmetric parts.

4.2 Displacement Field II

As mentioned already, the macroscopic variables will be split up into a symmetric and anti-symmetric part. This was also done in the previous Chapter, and from that it was seen that the symmetric part of the strain is the classical linear strain tensor (3.7). Regarding the stresses, it was clear that for isotropic elastic material behaviour, the symmetric part of the stress tensor is related to symmetric part of the strain tensor via Hooke's law (3.14). First, the definitions between the macroscopic and microscopic quantities are given. Then, the displacement field is derived using a potential energy approach.

4.2.1 The Relation between Microscopic and Macroscopic Quantities

Again, definitions must be given from which the relation between the macroscopic stresses and strains can be obtained. These definitions are

$$\bar{u}_i = \frac{1}{V} \int_R u_i \, \mathrm{d}\boldsymbol{y}, \tag{4.19}$$

$$\bar{\varphi}_i = \frac{1}{V} \int_R \varphi_i \, \mathrm{d}\boldsymbol{y}, \qquad \text{with} \quad \epsilon_{ijk} \varphi_k = \frac{1}{2} \left(\frac{\partial u_j}{\partial y_i} - \frac{\partial u_i}{\partial y_j} \right), \tag{4.20}$$

$$\frac{1}{2}(\bar{\varepsilon}_{ji} + \bar{\varepsilon}_{ij}) = \frac{1}{V} \int_R \varepsilon_{ji} \, \mathrm{d}\boldsymbol{y}, \tag{4.21}$$

$$\bar{\kappa}_{ji} = \frac{1}{V} \int_R \kappa_{ji} \, \mathrm{d}\boldsymbol{y}, \qquad \text{with} \quad \kappa_{ji} = \frac{\partial \varphi_i}{\partial y_j}, \tag{4.22}$$

$$\frac{1}{2}(\bar{\sigma}_{ji} + \bar{\sigma}_{ij}) = \frac{1}{V} \int_R \sigma_{ji} \, \mathrm{d}\boldsymbol{y}, \tag{4.23}$$

$$\bar{\mu}_{ji} = \frac{1}{V} \int_R \mu_{ji} \, \mathrm{d}\boldsymbol{y}, \qquad \text{with} \quad \mu_{ji} = \epsilon_{ilk} y_l \sigma_{jk}. \tag{4.24}$$

To arrive at a displacement field, we will start with the definitions of the macroscopic stresses and couple-stresses using the potential energy. Note that the boundary conditions will be a result of the

definitions given above. At this moment, we do not have any definitions regarding the skew-symmetric parts of the stress and strain tensors.

4.2.2 Potential Energy Approach

The definition of the macroscopic potential energy (4.16) allows us to relate the macroscopic stress and couple stresses to the microscopic stresses and 'couple stresses'. These relations then can be used to obtain relations between the macroscopic and microscopic deformation quantities. This can be achieved by writing out the equations for the stresses and couple stresses, which hold for all stress values. These obtained partial differential equations then can be solved for the microscopic strains. These strains subsequently will be used to arrive at the displacement fields.

As a starting point, we use expression (4.17) for the macroscopic stress. Then, with (4.23), we have

$$\frac{1}{2}\int_R \sigma_{lk}\left(\frac{\partial \varepsilon_{lk}}{\partial \bar{\varepsilon}_{ji}} + \frac{\partial \varepsilon_{lk}}{\partial \bar{\varepsilon}_{ij}}\right)\,\mathrm{d}\boldsymbol{y} = \int_R \sigma_{ji}\,\mathrm{d}\boldsymbol{y}. \tag{4.25}$$

Note that both σ_{ji} and ε_{ji} are symmetric. For the couple stresses, we use (4.18) with the definition (4.24),

$$\int_R \sigma_{lk}\frac{\partial \varepsilon_{lk}}{\partial \bar{\kappa}_{ji}}\,\mathrm{d}\boldsymbol{y} = \int_R \epsilon_{ilk} y_l \sigma_{jk}\,\mathrm{d}\boldsymbol{y}. \tag{4.26}$$

Note that these equations hold for all values of the stresses σ_{ji}. We will write out these equations for the two-dimensional case, taking the sum over repeated indices. The three equations for the stresses for (j,i)= (1,1), (1,2) and (2,2), and the two equations for (j,i) = (1,3) and (2,3) for the couple stresses are given by, respectively,

$$\int_R \left[\sigma_{11}\left(\frac{\partial \varepsilon_{11}}{\partial \bar{\varepsilon}_{11}} - 1\right) + \sigma_{12}2\frac{\partial \varepsilon_{12}}{\partial \bar{\varepsilon}_{11}} + \sigma_{22}\frac{\partial \varepsilon_{22}}{\partial \bar{\varepsilon}_{11}}\right]\mathrm{d}\boldsymbol{y} = 0, \tag{4.27}$$

$$\int_R \left[\sigma_{11}\frac{1}{2}\left(\frac{\partial \varepsilon_{11}}{\partial \bar{\varepsilon}_{21}} + \frac{\partial \varepsilon_{11}}{\partial \bar{\varepsilon}_{12}}\right) + \sigma_{12}\left(\frac{\partial \varepsilon_{12}}{\partial \bar{\varepsilon}_{21}} + \frac{\partial \varepsilon_{12}}{\partial \bar{\varepsilon}_{12}} - 1\right) + \sigma_{22}\frac{1}{2}\left(\frac{\partial \varepsilon_{22}}{\partial \bar{\varepsilon}_{21}} + \frac{\partial \varepsilon_{22}}{\partial \bar{\varepsilon}_{12}}\right)\right]\mathrm{d}\boldsymbol{y} = 0, \tag{4.28}$$

$$\int_R \left[\sigma_{11}\frac{\partial \varepsilon_{11}}{\partial \bar{\varepsilon}_{22}} + \sigma_{12}2\frac{\partial \varepsilon_{12}}{\partial \bar{\varepsilon}_{22}} + \sigma_{22}\left(\frac{\partial \varepsilon_{22}}{\partial \bar{\varepsilon}_{22}} - 1\right)\right]\mathrm{d}\boldsymbol{y} = 0, \tag{4.29}$$

$$\int_R \left[\sigma_{11}\left(\frac{\partial \varepsilon_{11}}{\partial \bar{\kappa}_{13}} + y_2\right) + \sigma_{12}2\left(\frac{\partial \varepsilon_{12}}{\partial \bar{\kappa}_{13}} - \frac{1}{2}y_1\right) + \sigma_{22}\frac{\partial \varepsilon_{22}}{\partial \bar{\kappa}_{13}}\right]\mathrm{d}\boldsymbol{y} = 0, \tag{4.30}$$

$$\int_R \left[\sigma_{11}\frac{\partial \varepsilon_{11}}{\partial \bar{\kappa}_{23}} + \sigma_{12}2\left(\frac{\partial \varepsilon_{12}}{\partial \bar{\kappa}_{23}} + \frac{1}{2}y_2\right) + \sigma_{22}\left(\frac{\partial \varepsilon_{22}}{\partial \bar{\kappa}_{23}} - y_1\right)\right]\mathrm{d}\boldsymbol{y} = 0. \tag{4.31}$$

Because these five equations hold for all stresses, the coefficients of σ_{11}, σ_{12} and σ_{22} have to vanish. This results in

$$\varepsilon_{11} = \bar{\varepsilon}_{11} - \bar{\kappa}_{13}y_2, \tag{4.32}$$

$$\varepsilon_{22} = \bar{\varepsilon}_{22} + \bar{\kappa}_{23}y_1, \tag{4.33}$$

$$\varepsilon_{12} = \frac{1}{2}(\bar{\varepsilon}_{12} + \bar{\varepsilon}_{21}) + \frac{1}{2}\bar{\kappa}_{13}y_1 - \frac{1}{2}\bar{\kappa}_{23}y_2. \tag{4.34}$$

Integrating (4.32) with respect to y_1 and (4.33) with respect to y_2, yields

$$u_1 = \bar{\varepsilon}_{11}y_1 - \bar{\kappa}_{13}y_1y_2 + g(y_2), \tag{4.35}$$

$$u_2 = \bar{\varepsilon}_{22}y_2 - \bar{\kappa}_{23}y_1y_2 + f(y_1). \tag{4.36}$$

When we calculate ε_{12} of these displacements and equal this result with (4.34), we have

$$-\bar{\kappa}_{13}y_1 + g'(y_2) + \bar{\kappa}_{23}y_2 + f'(y_1) = \bar{\varepsilon}_{12} + \bar{\varepsilon}_{21} + \bar{\kappa}_{13}y_1 - \bar{\kappa}_{23}y_2, \tag{4.37}$$

where $'$ represents differentiation with respect to its argument. Rearranging this equation with y_1-terms to the left-hand side of the equal sign, and y_2-terms to the right-hand side, and noting that the left-hand side can only be equal to the same constant, α say, and integrating, we have,

$$f(y_1) = u_{02} + \alpha y_1 + \frac{1}{2}(\bar{\varepsilon}_{12} + \bar{\varepsilon}_{21})y_1 + \bar{\kappa}_{13}y_1^2, \tag{4.38}$$

$$g(y_2) = u_{01} - \alpha y_2 + \frac{1}{2}(\bar{\varepsilon}_{12} + \bar{\varepsilon}_{21})y_2 - \bar{\kappa}_{23}y_2^2, \tag{4.39}$$

where u_{01} and u_{02} are integration constants. Finally, substituting these results in (4.35) and (4.36), we obtain the expressions for the boundary conditions, which are consistent with the definitions of the symmetric part of the stress tensor and the strain tensor,

$$u_1 = u_{01} - \alpha y_2 + \bar{\varepsilon}_{11}y_1 + \frac{1}{2}(\bar{\varepsilon}_{12} + \bar{\varepsilon}_{21})y_2 \qquad -\bar{\kappa}_{13}y_1y_2 - \bar{\kappa}_{23}y_2^2, \tag{4.40}$$

$$u_2 = u_{02} + \alpha y_1 + \bar{\varepsilon}_{22}y_2 + \frac{1}{2}(\bar{\varepsilon}_{12} + \bar{\varepsilon}_{21})y_1 + \bar{\kappa}_{13}y_1^2 + \bar{\kappa}_{23}y_1y_2. \tag{4.41}$$

Note that α can be explained as a rigid rotation, and u_{01} and u_{02} as rigid displacements. Note also, that these boundary conditions are quite simular to those given in the preceding Section. In the next Section, the parameters in the proposed constitutive equations will be fitted using the derived boundary conditions.

4.3 Determining the Macroscopic Constitutive Equations

A study was carried out regarding the isotropy of the RVE. A tensile test and a shear test were applied to the RVE. From both tests, the shear modulus was calculated, using the appropriate plane strain equations for isotropic elastic material behaviour. The deviation between both results for the shear modulus was well within 1%, so the RVE can be modelled as isotropic, which justifies choosing the constitutive equations given in the preceding Chapter. By defining Young's modulus as a non-linear function of an equivalent strain measure, strain softening behaviour can be incorporated. The parameters used in these equations now have to be fitted onto finite element calculations on the RVE, which is depicted in Fig.1.3(a). Applying the boundary conditions derived in the preceding Section on the RVE, will result in stresses and moments in the RVE, which will be averaged over the RVE. The evolutions of the averaged values which, by definition, correspond to the macroscopic quantities, are used to fit the macroscopic parameters. Note that the parameter ϑ can not be fitted, since the anti-symmetric part is not included in the formulation.

The matrix material is modelled using the compressible Leonov model with polycarbonate parameters, as was mentioned in the Introduction, whereas the 'hole' is assumed isotropic elastic with a modulus of $E = 1$ and $\nu = 0.03$.

Two tests have to be performed on the RVE to fit the parameters. The first is a true tensile test and the second is a bending test.

Tensile Test

This test is applied to the RVE for fitting Poission's ratio and Young's modulus. The boundary conditions result in $\bar{\sigma}_{22} = 0$. Using this in the constitutive equations, an expression for Poisson's ratio will be obtained. Substitution of this equation into the constitutive equations will result in an expression for Young's modulus.

The tensile test is applied to the RVE by prescribing uniform displacements on $y_1 = \pm a$. The applied (constant) strain rate is $\dot{\varepsilon} = 10^{-2}\,s^{-1}$. Because of symmetry, only one quarter of the RVE has to be

modelled (Fig.1.3). The tractions $\boldsymbol{t}$ on $y_2 = a$ vanish. The boundary conditions now read

$$u_1(a, y_2) = \bar{\varepsilon}_{11}\, a, \qquad \text{on } y_1 = a, \tag{4.42}$$

$$t_2(y_1, a) = 0 \qquad \text{on } y_2 = a. \tag{4.43}$$

The deformed RVE is depicted in Fig.1.3(b). The averaged stresses $\bar{\sigma}_{11}$ and $\bar{\sigma}_{22}$ can be determined from the reaction forces on the boundaries. The averaged strains $\bar{\varepsilon}_{11}$ and $\bar{\varepsilon}_{22}$ can be determined from the displacements on the boundaries. Since the E-modulus is a function of the equivalent strain in the macroscopic model defined by (3.45), the averaged equivalent strain also has to be calculated from the values of the averaged strains, according to (3.51).

In Fig.4.1, the averaged strains and stresses are depicted as functions of the equivalent strain.

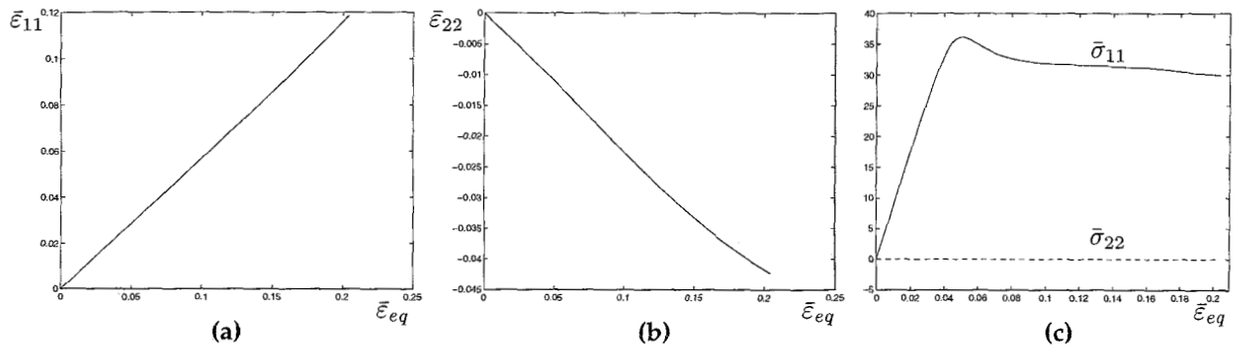

Figure 4.1: The averaged normal strain(a), transversal strain(b) and stresses in [MPa](c) during deformation

From Fig.4.1(c), the typical strain softening behaviour of $\bar{\sigma}_{11}$ can be noticed, whereas it can be seen that $\bar{\sigma}_{22}$= 0 is confirmed. Then, the constitutive equation (3.47) for $\bar{\sigma}_{22} = 0$ yields the following expression for Poisson's ratio,

$$\bar{\nu} = -\frac{\bar{\varepsilon}_{22}}{\bar{\varepsilon}_{11} - \bar{\varepsilon}_{22}}. \tag{4.44}$$

This relation can be used to determine $\bar{\nu}$ as a function of $\bar{\varepsilon}_{eq}$ and is depicted in the solid line in Fig.4.2(a).

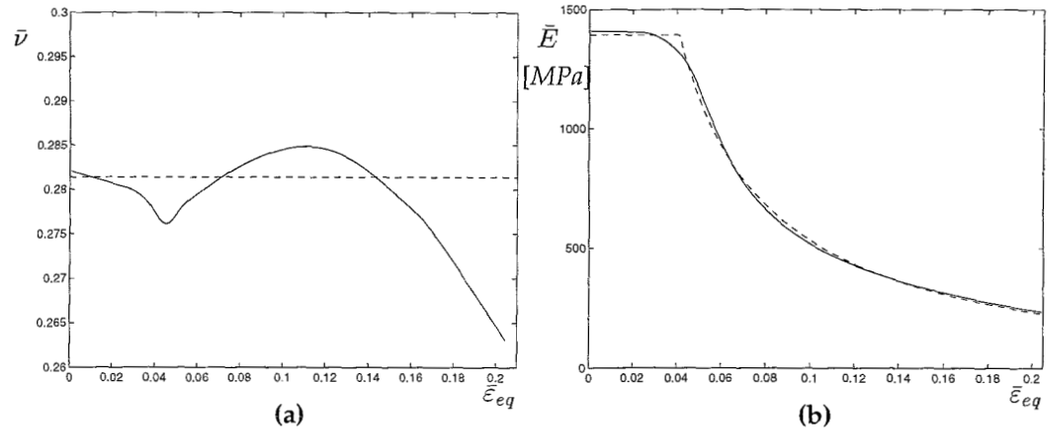

Figure 4.2: The calculated (solid lines) and the fitted (dashed lines) values of (a) Poission's ratio and (b) Young's modulus as functions of the equivalent strain

When substituting (4.44) into (3.47) for $\bar{\sigma}_{11}$, we obtain a relation for the $\bar{E}$-modulus,

$$\bar{E} = (1 - \bar{\nu}^2)\frac{\bar{\sigma}_{11}}{\bar{\varepsilon}_{11}}. \tag{4.45}$$

This relation can be used to determine $\bar{E}$ as a function of the equivalent strain and is depicted in Fig.4.2(b). The fitted (dashed) lines are also shown for $\bar{\nu}$ and $\bar{E}$.

In addition, it can be observed that the variation of $\bar{\nu}$ is small (a value between 0.288 and 0.26), so the influence of this variation seems quite negligible. The dashed line in Fig.4.2(a) shows that $\bar{\nu}$ is fitted as a constant value. The reason for this is that in the proposed constitutive equations, $\bar{\nu}$ is also constant. This justifies the choice of a constant value for $\bar{\nu} = 0.2814$, which is obtained from a least squares algorithm. The averaged function of the E-modulus is fitted, as illustrated in Fig.4.2(b). The fitted function is given by (3.45) with unknown values for E_0, ζ and ε_0. These values are also obtained from a least squares fitting procedure, which resulted in the values: $E_0 = 1393.57$ [MPa], $\zeta = 0.0464$ and $\varepsilon_0 = 0.0409$.

Bending Test

The purpose of the bending test is to determine the parameter $\bar{P}$. The curvature $\bar{\kappa}_{13}$ will be used to prescribe the displacements on the boundaries $y_1 = \pm a$. For the same purpose, $\bar{\kappa}_{23}$ could be prescribed, since the RVE is assumed isotropic. In addition, the tractions on $y_2 = \pm a$ vanish.

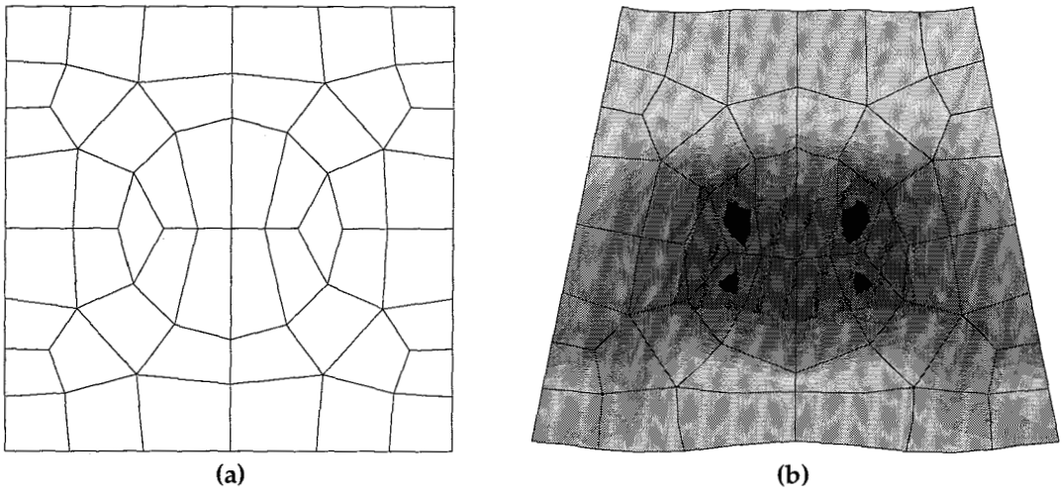

(a) (b)

Figure 4.3: (a) The undeformed and (b) the deformed mesh of the bending test on the RVE

The boundary conditions now read

$$u_1(\pm a, y_2) = \mp \bar{\kappa}_{13}\, a\, y_2, \tag{4.46}$$

$$u_2(\pm a, y_2) = \bar{\kappa}_{13}\, a^2 \qquad \text{on } y_1 = \pm a, \tag{4.47}$$

$$t_2(y_1, \pm a) = 0 \qquad \text{on } y_2 = \pm a. \tag{4.48}$$

The undeformed mesh and the deformed mesh of the RVE are depicted in Fig.4.3(a) and (b), respectively. Note that the used mesh is more coarse than the one depicted in Fig.1.3. The reason for this is minimizing the CPU-time, while still obtaining accurate results. A comparison study, where some displacement fields were applied on the RVE, revealed that the results from the two different meshes differ at most 10%.

The calculations showed that $\bar{\varepsilon}_{11}$ equals zero. The transversal strain does not vanish (Fig.4.4(a)). More specifically, this value of $\bar{\varepsilon}_{22}$ and of $\bar{\sigma}_{11}$ (Fig.4.4(b)), which should vanish as well since ideally, $\bar{\sigma}_{11}$

is linear in y_2, are an indication of the error made by the application of the proposed constitutive model. From this model, it is expected that, when both $\bar{\sigma}_{22}$ and $\bar{\varepsilon}_{11}$ vanish, $\bar{\varepsilon}_{22}$ should vanish too (3.47). The typical strain softening behaviour can be recognized in Fig.4.4(c).

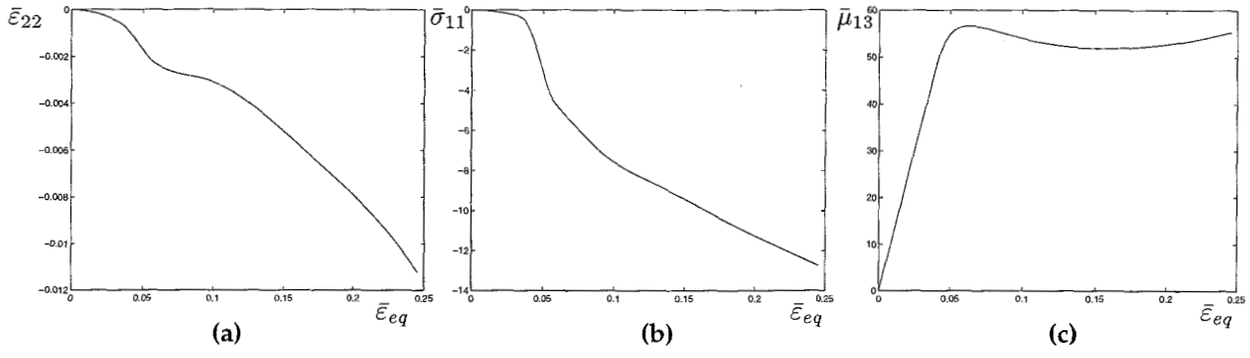

Figure 4.4: The averaged transversal strain (a), normal stress in [MPa] (b) and couple stress in [MPa.m] (c) during deformation

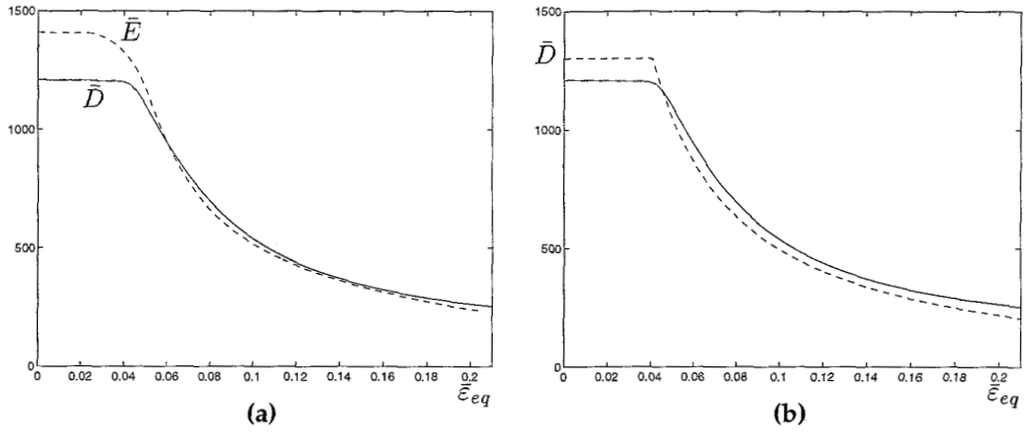

Figure 4.5: (a) The relation between the modulus (dashed line) and the bending modulus (solid line) and (b) the calculated bending modulus (solid line) with the fitted curve of the bending modulus (dashed line)

Observing the resemblance between Fig.4.5(c) and Fig.4.2(c), and more specifically, between the two curves of Fig.4.5(a), we may fit $\bar{P}$ using the equation for the E-modulus. From (3.47), it holds that

$$\bar{\mu}_{13} = \bar{E}\ell^2\bar{P}\bar{\kappa}_{13} = \bar{D}\bar{\kappa}_{13}, \tag{4.49}$$

where we define $\bar{D}$ as the *bending modulus*. Thus, the relations between the stresses and strains on one hand, and the couple stresses and curvatures on the other hand, are identical, except for a constant $\ell^2\bar{P}$, where ℓ equals the size of the RVE (=1). This is illustrated in Fig.4.5(a), where both the bending modulus from the bending test and the E-modulus from the tensile test are depicted. Note that these curves are the results of the finite element calculations on the RVE. The resemblance between the two curves is evident. Thus, we may fit $\bar{D}$ with the same function as the one we used for $\bar{E}$. The fitted result is given in Fig.4.5(b). The fitted curve is obtained by using the given relation of the E-modulus, with the values for ζ and ε_0 from the fitting results of the tensile test. However, instead of using E_0, we fitted $\bar{P}$ (4.49). Again, using a least squares algorithm, we obtain the value for this constant: 0.9334. In the next Section we substitute these values into the existing finite element program. For clearance, we give an overview of the fitted results in Table 4.1.

		$E = E_0\left[(1+\zeta)\frac{\varepsilon_0}{\varepsilon_{eq}} - \zeta\right]$		
$\bar{\nu}$ [-]	P [-]	E_0 [MPa]	ζ [-]	ε_0 [-]
0.2814	0.9334	1393.57	0.0464	0.0409

Table 4.1: Results of the fitting procedure

4.4 Applications

In this Section, we will discuss three applications, a tensile test, a shear test, both similar to the tests of the previous Chapter, and a tensile test on a nodged specimen. In these simulations, the parameters used in the constitutive equations are the values obtained from the fitting procedures, i.e. the homogenized values (Table 4.1). The chosen value for ϑ in all simulations equals 0.8.

4.4.1 Tensile Test

First, a tensile test is carried out on a specimen with dimensions $20a \times 2a$, with a the size of the RVE. The specimen and the boundary conditions have already been shown in Fig.3.8(a). Results from this test for two different finite element discretizations are shown in Fig.4.6. It appears that the solution is mesh-independent.

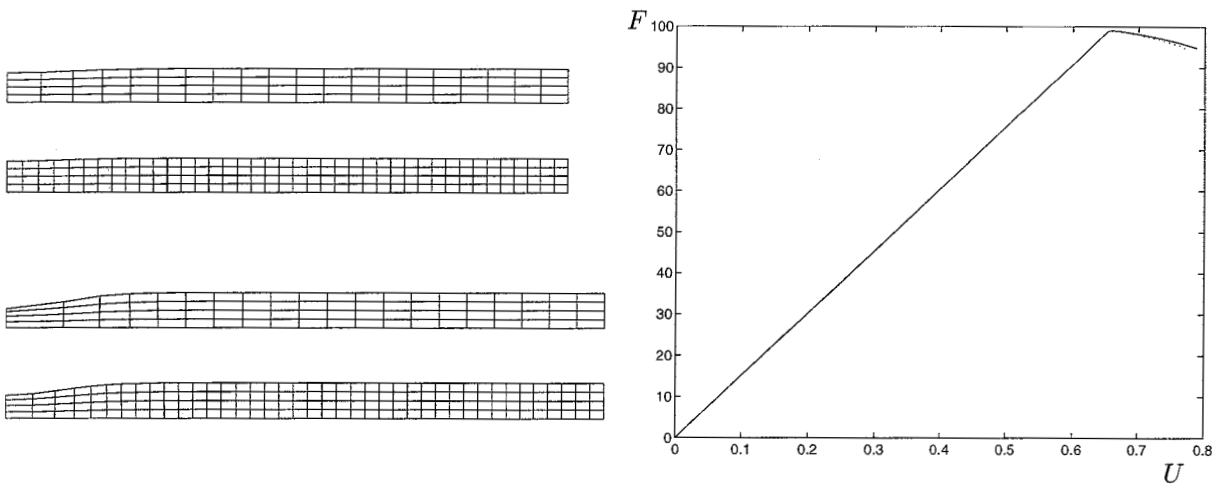

Figure 4.6: Two deformation stages for the meshes of 80 and 160 elements and the resulting load-displacement curves (solid: 80 elements; dotted: 160 elements)

To illustrate the effect of strain hardening, we will artificially set the hardening parameter, $\chi = +\zeta$ and $\varepsilon_1 = 0.25$. Note that these values do not result from the fitting procedure. The deformation stages are depicted in Fig.4.7, and to illustrate the typical hardening behaviour, the equivalent stress versus equivalent strain is also shown.

4.4.2 Shear Test

As a second application, a shear test, similar to the one in the preceding Chapter, will be described. The dimensions of the specimen are $a \times 40a$, where a represents the size of the RVE. The boundary conditions are analog to the test in the preceding Chapter.

Here also, the fitted parameters are used in the constitutive model, which results in the deformation stages and a load-displacement curve depicted in Fig.4.8 and Fig.4.9, respectively. A localization zone

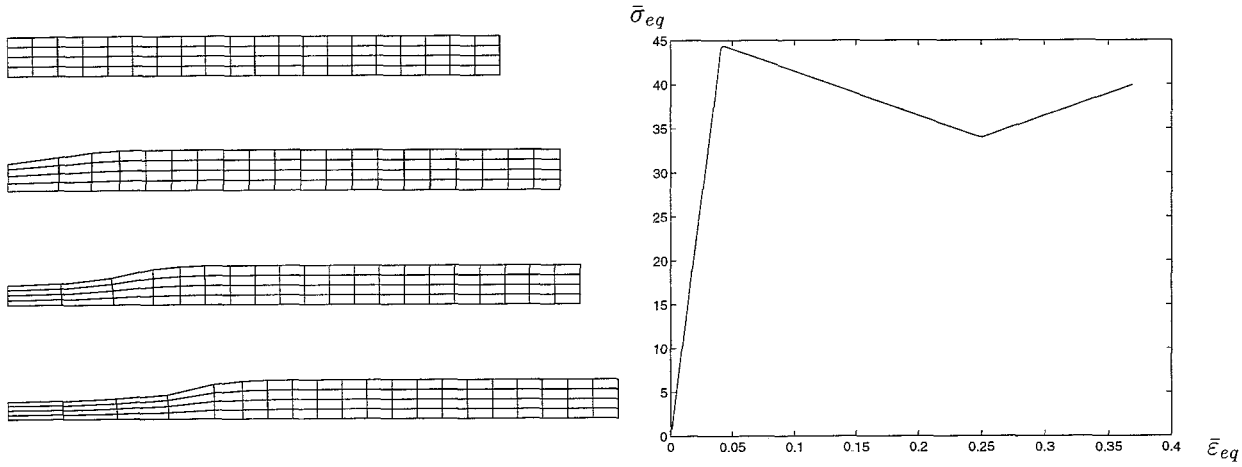

Figure 4.7: Deformation stages of the macroscopic tensile specimen with hardening and the equivalent stress versus equivalent strain

emerges in the centre of the specimen, caused by the non-homogeneous strain distribution over the test specimen. It appears that this localization zone is mesh-independent.

4.4.3 Tensile Test on a Nodged Specimen

As a final application, we will show a tensile test on a single-edged nodged strip. The specimen and the boundary conditions are shown in Fig.4.10. The resulting force-displacement curves for two different discretizations are shown in Fig.4.11. Two deformation stages of the different meshes are illustrated in Fig.4.12.

It is necessary to validate these results with results obtained from macroscopic simulations and existing homogenization methods. Only then, it will be possible to draw conclusions about the correctness of the obtained results.

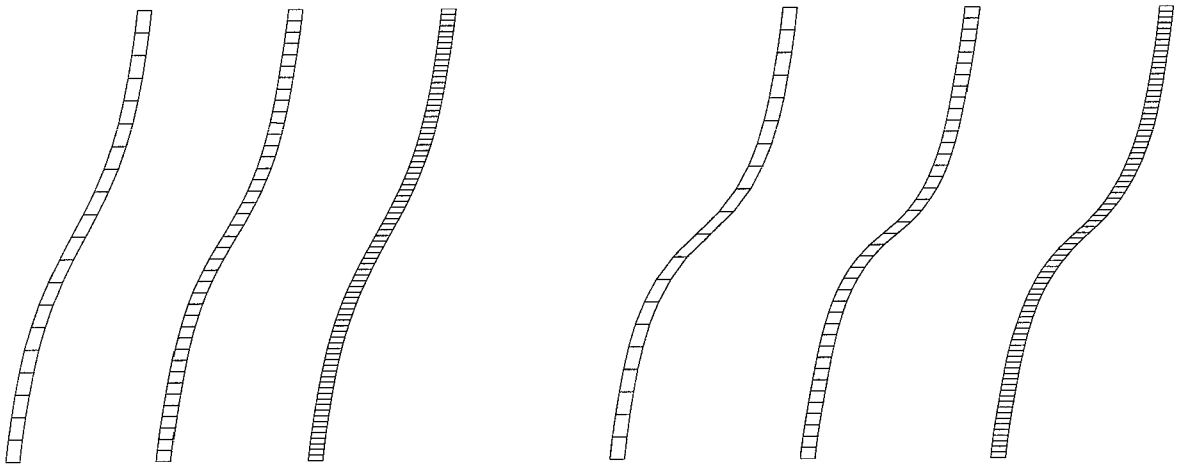

Figure 4.8: Deformation stages of the shear test for the different finite element meshes of 20, 40 and 80 elements

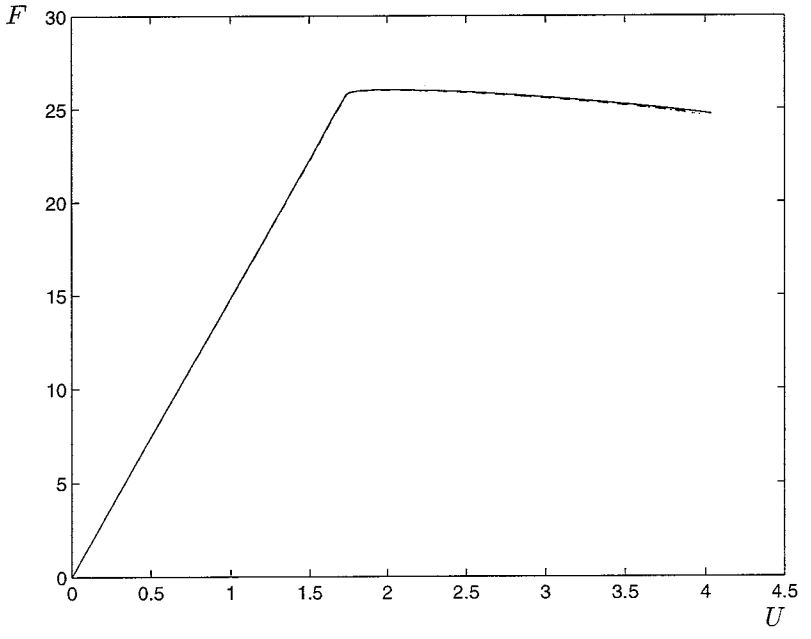

Figure 4.9: The load-displacement curve for the different meshes: 20 elements (solid), 40 elements (dotted) and 80 element (dashed)

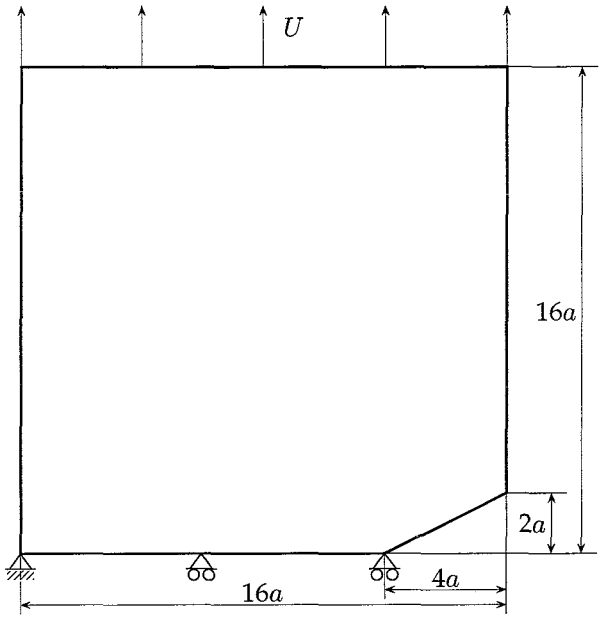

Figure 4.10: The single edge nodged specimen loaded in tensile

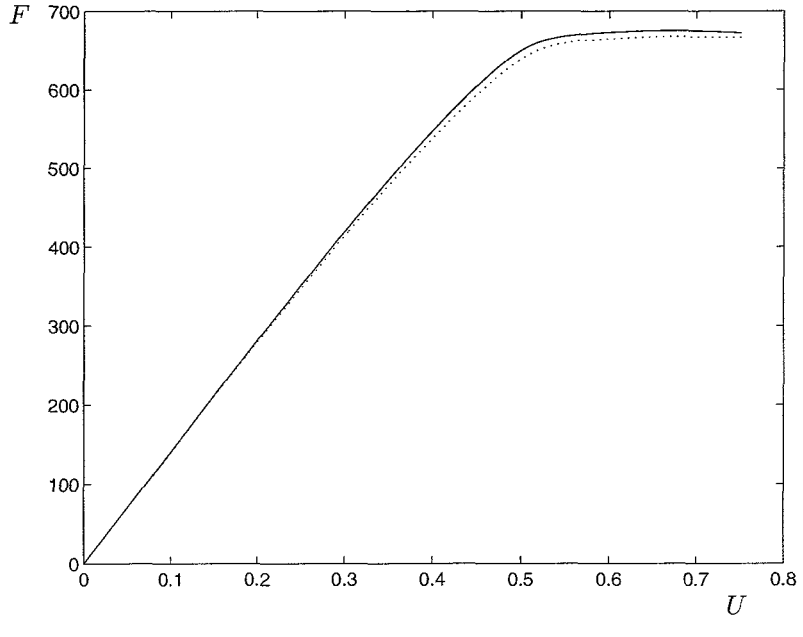

Figure 4.11: The resulting load-displacement curves for the coarse (solid) and the fine (dotted) mesh

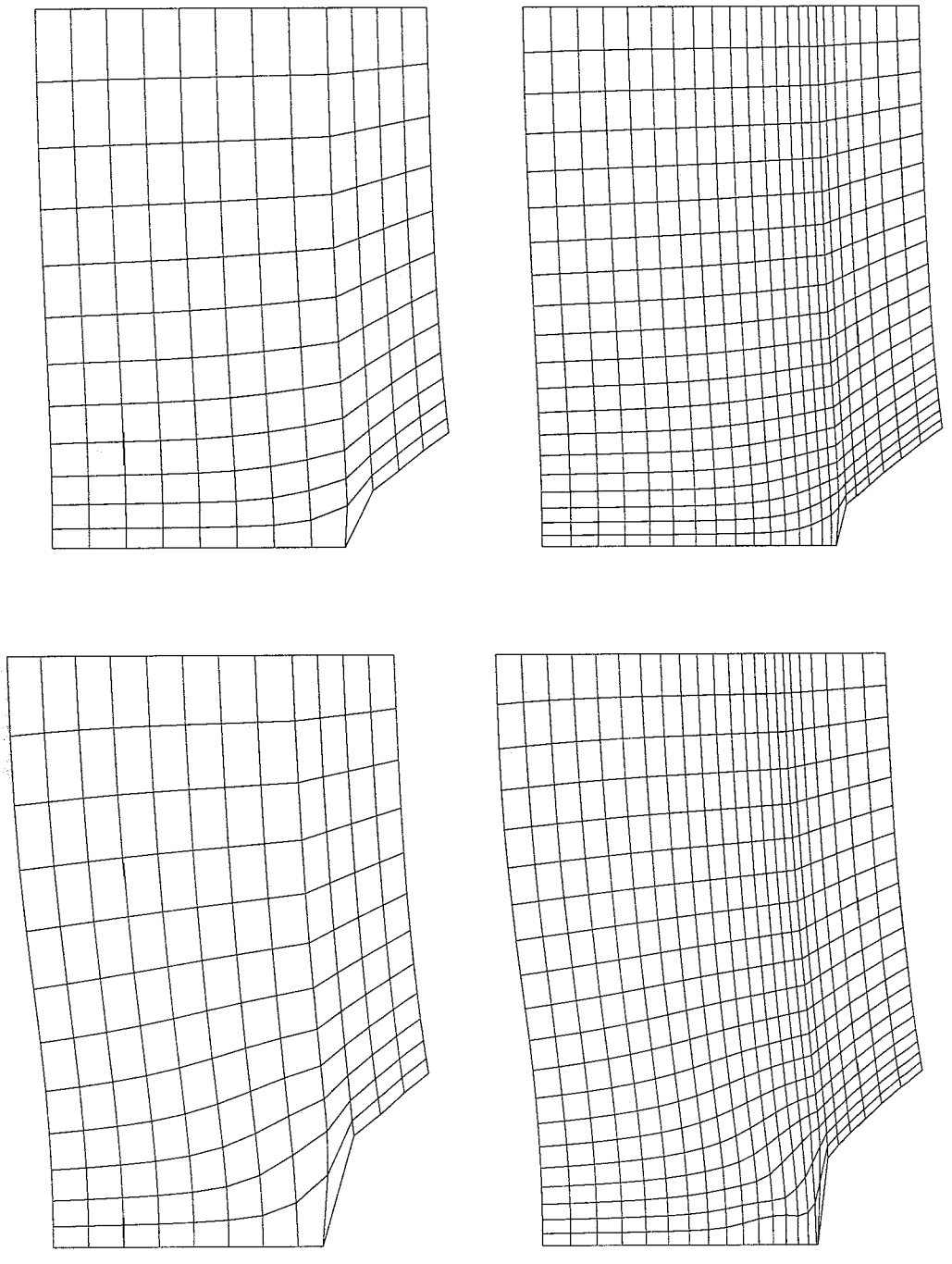

Figure 4.12: Deformation stages of the tensile test on a nodged specimen for two finite element meshes

5 Discussion

The objective of this report was to devise constitutive equations for heterogeneous polymers based on micromechanics using homogenization procedures. For this purpose, a polycarbonate plate with holes was taken as a model material. The mechanical behaviour of the polycarbonate was modelled using a compressible Leonov model. Since this material exhibits localization of deformation, standard homogenization methods which relate averages of the stress to averages of the strain over a representative part of the material (RVE), cannot be applied to derive a macroscopic constitutive equation. Instead, the material description has to be supplemented with additional information.

In Chapter 2, the homogenization process was discussed. The additional degrees of freedom discussed in this Chapter were partial derivatives of the macroscopic strain field. These were defined as averages of partial derivatives of the microscopic strain field. To obtain the relation between these macroscopic deformation quantities and the macroscopic stresses, which were defined as averages of the microscopic stresses, the former had to be applied to the RVE by means of appropriate boundary conditions. The influence of the size of the RVE and its position in the macroscopic material on these boundary conditions was illustrated with some examples.

To arrive at a closed form constitutive equation, the macroscopic stress was assumed to be a function of the macroscopic strain and the Laplacian of the macroscopic strain only. This function was obtained by expanding the stress into a Taylor series of which the parameters have to be determined. To this end, a large number of simulations should have to be carried out. Since this will result in large CPU-times, a more heuristical approach in the formulation of the constitutive equations is desired. It appeared that Cosserat theory provides the desired additional quantities being rotational degrees of freedom.

In Chapter 3 Cosserat theory was described. The deformation and constitutive variables appeared to be not symmetric. It was shown that the symmetric part of the Cosserat strain tensor was identical to the classical linear strain tensor. The finite element formulation of the Cosserat theory was devised assuming the two-dimensional plane strain case. As an example of strain softening behaviour, the constitutive equations were formulated as a non-linear function of the deformation. This was achieved by defining the elasticity modulus as a function of an equivalent strain. The simulations with this model showed that the element was capable of describing strain softening behaviour in a proper way. However, this capability strongly depended on the choice of the material parameters. It might be worthwile expanding the formulation to three dimensions. This will add more degrees of freedom of the macroscopic model and therefore its capability of describing strain softening behaviour might improve.

The homogenization of the model material was discussed in Chapter 4. Here, definitions were made relating the macroscopic Cosserat and microscopic deformation variables on one hand, and the microscopic and macroscopic constitutive quantities on the other hand. The definitions of the symmetrical parts of the stress and strain tensor were given. In addition, the definitions of the curvatures and couple stresses were shown. These relations between the microscopic and macroscopic quantities have an influence on the result of the homogenization process, that is, on the macroscopic constitutive equations. In order to obtain the macroscopic constitutive equations, consistent boundary conditions in terms of the macroscopic deformation quantities, are applied to the RVE by means of a derived displacement field. These boundary conditions resulted in a non-periodic deformation of the RVE.

The parameters used in the macroscopic constitutive equations were fitted onto finite element calculations by applying two different displacement fields to the RVE. The parameter defining the skew-symmetric part could not be determined by the lack of definitions of this part. The averaging of the microscopic quantities in the bending test revealed that some variables did not vanish, which was in conflict with the prescribed boundary conditions. This can be seen as an indication of the error of the chosen macroscopic constitutive model.

Since the RVE was loaded to a strain at which no hardening occured, strain hardening behaviour of the macroscopic model was excluded. However, this can be included by applying a sufficient load to the RVE. It was shown by including artificial strain hardening, which was not the result of the fitting procedure, that the localization of deformation and the consequent neck propagation was described properly. To arrive at more realistic results, the macroscopic formulation has to be extended to large de-

formations. In addition, an elasto-plastic formulation has to be included. Since the microscopic Leonov model is history dependent, the macroscopic model should also be able of capturing this characteristic behaviour. The possibility of expanding the description to so-called micro-morphic models should also be mentioned. This can be explained as an extension of the Cosserat theory.

The results of the applications should be validated with macroscopic simulations or with results from other homogenization techniques. As a final recommendation, the influence of the RVE, like hole radius, hole stacking and hole size, on the macroscopic behaviour should be studied.

Bibliography

Auriault, J. L. (1991). Heterogeneous medium. Is an equivalent macroscopic description possible? *International Journal of Science and Engineering*, **29**(7), 785–795.

Baaijens, F. (1994). *Applied Computational Mechanics*. Syllabus, Eindhoven University of Technology.

Beran, M. J. (1968). *Statistical Continuum Theories*, volume 9 of *Monographs in Statistical Physics and Thermodynamics*. Interscience Publishers, New York.

Boutin, C. (1996). Microstructural effects in elastic solids. *International Journal of Solids and Structures*, **33**(7), 1023–1051.

Coomans, A. (1995). Experimental analysis of the deformation behaviour of polycarbonate plate with macroscopic holes (in dutch). EUT-report 95–038, Eindhoven University of Technology, Eindhoven.

De Borst, R. (1990). Simulation of localisation using cosserat theory. In N. Bićanić and H. Mang, editors, *Computer Aided Analysis and Design of Concrete Structures*, volume 2, pages 931–943, Swansea, United Kingdom. Pineridge Press. Proceedings of SCI-C 1990, Second International Conference held in Zell am See, Austria.

De Borst, R. and Mühlhaus, H.-B. (1991). Continuum models for discontinuous media. In J. van Mier, J. Rots, and A. Bakker, editors, *Fracture Processes in Concrete, Rock and Ceramics*, volume 2, pages 601–618, London, United Kingdom. E & FN Spon. Proceedings of the International RILEM/ESIS conference, Noordwijk, The Netherlands, June 19–21, 1991.

Gdoutos, E. (1993). *Fracture Mechanics : An Introduction*. Kluwer Academic Publishers.

Ghosh, S. and Moorthy, S. (1995). Elastic-plastic analysis of arbitrary heterogeneous materials with the voronoi cell finite element method. *Computer Methods in Applied Mechanics and Engineering*, **121**(1-4), 373–409.

Ghosh, S., Lee, K., and Moorthy, S. (1995). Multiple scale analysis of heterogeneous elastic structures using homogenization theory and voronoi cell finite element method. *International Journal of Solids and Structures*, **32**(1), 27–62.

Hollister, S. and Kikuchi, N. (1992). A comparison of homogenization and standard mechanics analyses for periodic porous composites. *Computational Mechanics*, **10**, 73–95.

Logan, D. (1992). *A First Introduction in the Finite Element Method*. PWS-Kent Publishing Company, Boston.

Mura, T. (1987). *Micromechanics of Defects in Solids*. Martinus Nijhoff, Dordrecht.

Nemat-Nasser, S. and Hori, M. (1993). *Micromechanics: Overall Properties of Heterogeneous Materials*. Elsevier Science Publishers.

Nowacki, W. (1986). *Theory of Asymmetric Elasticity*. Pergamon Press/PWN Polish Scientific Publishers, Warsawa/Oxford.

Smit, R. (1994). Numerical simulation of localization phenomena in polymer glasses. EUT-report 94–046, Eindhoven University of Technology.

Smit, R. and Timmermans, P. (1995). *Implementation of the compressible Leonov model with hardening in Marc*. Personal notes.

Triantafyllidis, N. and Aifantis, E. (1986). A gradient approach to localization of deformation. i. hyperelastic materials. *Journal of Elasticity*, **16**, 225–237.

Tvergaard, V. and Needleman, A. (1995). Effects of non-local damage in porous plastic solids. *International Journal of Solids and Structures*, **32**(8/9), 1063–1077.

Van der Sanden, M. (1993). *Ultimate Toughness of Amorphous Polymers*. Ph.D. thesis, Eindhoven University of Technology, Eindhoven.

Vosbeek, P. (1994). *A Micromechanical Approach to Deformation and Failure of Discrete Media*. Ph.D. thesis, Eindhoven University of Technology, Eindhoven.

Vosbeek, P. (1996). *Homogenisation of Heterogeneous Media*. Personal notes.

Zienkiewicz, O. (1977). *The Finite Element Method*. McGraw-Hill Book Company, London.

A Component Form of the Displacement Field

The displacement field (2.27) can be written out as follows:

$$
\begin{aligned}
u_1 = \; & u_{01} + \bar{\varepsilon}_{11} y_1 + \bar{\varepsilon}_{12} y_2 + \frac{1}{2}\left(\frac{\partial \bar{\varepsilon}_{11}}{\partial x_1} y_1^2 + \frac{\partial \bar{\varepsilon}_{11}}{\partial x_2} y_1 y_2 + \frac{\partial \bar{\varepsilon}_{12}}{\partial x_1} y_1 y_2 + \frac{\partial \bar{\varepsilon}_{12}}{\partial x_2} y_2^2\right) \\
& + \frac{1}{6}\left(\frac{\partial^2 \bar{\varepsilon}_{11}}{\partial x_1^2} y_1^3 + 2\frac{\partial^2 \bar{\varepsilon}_{11}}{\partial x_1 \partial x_2} y_1^2 y_2 + \frac{\partial^2 \bar{\varepsilon}_{11}}{\partial x_2^2} y_1 y_2^2\right. \\
& + \left.\frac{\partial^2 \bar{\varepsilon}_{12}}{\partial x_1^2} y_1^2 y_2 + 2\frac{\partial^2 \bar{\varepsilon}_{12}}{\partial x_1 \partial x_2} y_1 y_2^2 + \frac{\partial^2 \bar{\varepsilon}_{12}}{\partial x_2^2} y_2^3\right) \\
& - \frac{1}{6} a^2 \left(\frac{\partial \bar{\varepsilon}_{11}}{\partial x_1} + \frac{\partial \bar{\varepsilon}_{12}}{\partial x_2} + \frac{\partial^2 \bar{\varepsilon}_{11}}{\partial x_1^2} y_1 + \frac{\partial^2 \bar{\varepsilon}_{12}}{\partial x_1^2} y_2 + \frac{\partial^2 \bar{\varepsilon}_{11}}{\partial x_2^2} y_1 + \frac{\partial^2 \bar{\varepsilon}_{12}}{\partial x_2^2} y_2\right)
\end{aligned}
\tag{A.1}
$$

$$
\begin{aligned}
u_2 = \; & u_{01} + \bar{\varepsilon}_{21} y_1 + \bar{\varepsilon}_{22} y_2 + \frac{1}{2}\left(\frac{\partial \bar{\varepsilon}_{21}}{\partial x_1} y_1^2 + \frac{\partial \bar{\varepsilon}_{21}}{\partial x_2} y_1 y_2 + \frac{\partial \bar{\varepsilon}_{22}}{\partial x_1} y_1 y_2 + \frac{\partial \bar{\varepsilon}_{22}}{\partial x_2} y_2^2\right) \\
& + \frac{1}{6}\left(\frac{\partial^2 \bar{\varepsilon}_{21}}{\partial x_1^2} y_1^3 + 2\frac{\partial^2 \bar{\varepsilon}_{21}}{\partial x_1 \partial x_2} y_1^2 y_2 + \frac{\partial^2 \bar{\varepsilon}_{21}}{\partial x_2^2} y_1 y_2^2\right. \\
& + \left.\frac{\partial^2 \bar{\varepsilon}_{22}}{\partial x_1^2} y_1^2 y_2 + 2\frac{\partial^2 \bar{\varepsilon}_{22}}{\partial x_1 \partial x_2} y_1 y_2^2 + \frac{\partial^2 \bar{\varepsilon}_{22}}{\partial x_2^2} y_2^3\right) \\
& - \frac{1}{6} a^2 \left(\frac{\partial \bar{\varepsilon}_{21}}{\partial x_1} + \frac{\partial \bar{\varepsilon}_{22}}{\partial x_2} + \frac{\partial^2 \bar{\varepsilon}_{21}}{\partial x_1^2} y_1 + \frac{\partial^2 \bar{\varepsilon}_{22}}{\partial x_1^2} y_2 + \frac{\partial^2 \bar{\varepsilon}_{21}}{\partial x_2^2} y_1 + \frac{\partial^2 \bar{\varepsilon}_{22}}{\partial x_2^2} y_2\right)
\end{aligned}
\tag{A.2}
$$

B Resulting Microscopic Displacement Fields

For clearness, some equations will be repeated here. The used linear strain measure is defined as

$$\bar{\varepsilon}_{ij} = \frac{1}{2}\left(\frac{\partial \bar{u}_i}{\partial x_j} + \frac{\partial \bar{u}_j}{\partial x_i}\right) = \begin{pmatrix} \frac{\partial \bar{u}_1}{\partial x_1} & \frac{1}{2}\left(\frac{\partial \bar{u}_1}{\partial x_2} + \frac{\partial \bar{u}_2}{\partial x_1}\right) \\ \frac{1}{2}\left(\frac{\partial \bar{u}_2}{\partial x_1} + \frac{\partial \bar{u}_1}{\partial x_2}\right) & \frac{\partial \bar{u}_2}{\partial x_2} \end{pmatrix} = \begin{pmatrix} \bar{\varepsilon}_{11} & \bar{\varepsilon}_{12} \\ \bar{\varepsilon}_{21} & \bar{\varepsilon}_{22} \end{pmatrix} \tag{B.1}$$

The first derivative, which we also need to formulate the displacement field, can be 'visualised' as a three-dimensional matrix, or a third-order tensor: $\partial \bar{\varepsilon}_{ij}/\partial x_k$. This matrix consists of two different 'layers', viz.

$$\frac{\partial \bar{\varepsilon}_{ij}}{\partial x_1} = \begin{pmatrix} \frac{\partial \bar{\varepsilon}_{11}}{\partial x_1} & \frac{\partial \bar{\varepsilon}_{12}}{\partial x_1} \\ \frac{\partial \bar{\varepsilon}_{21}}{\partial x_1} & \frac{\partial \bar{\varepsilon}_{22}}{\partial x_1} \end{pmatrix} \qquad \frac{\partial \bar{\varepsilon}_{ij}}{\partial x_2} = \begin{pmatrix} \frac{\partial \bar{\varepsilon}_{11}}{\partial x_2} & \frac{\partial \bar{\varepsilon}_{12}}{\partial x_2} \\ \frac{\partial \bar{\varepsilon}_{21}}{\partial x_2} & \frac{\partial \bar{\varepsilon}_{22}}{\partial x_2} \end{pmatrix} \tag{B.2}$$

Next, we need second order derivatives of the strain, $\partial^2 \bar{\varepsilon}_{ij}/\partial x_k \partial x_l$. This is a four dimensional matrix, or, a fourth order tensor:

$$\frac{\partial^2 \bar{\varepsilon}_{ij}}{\partial x_1^2} = \begin{pmatrix} \frac{\partial^2 \bar{\varepsilon}_{11}}{\partial x_1^2} & \frac{\partial^2 \bar{\varepsilon}_{12}}{\partial x_1^2} \\ \frac{\partial^2 \bar{\varepsilon}_{21}}{\partial x_1^2} & \frac{\partial^2 \bar{\varepsilon}_{22}}{\partial x_1^2} \end{pmatrix} \qquad \frac{\partial^2 \bar{\varepsilon}_{ij}}{\partial x_2^2} = \begin{pmatrix} \frac{\partial^2 \bar{\varepsilon}_{11}}{\partial x_2^2} & \frac{\partial^2 \bar{\varepsilon}_{12}}{\partial x_2^2} \\ \frac{\partial^2 \bar{\varepsilon}_{21}}{\partial x_2^2} & \frac{\partial^2 \bar{\varepsilon}_{22}}{\partial x_2^2} \end{pmatrix} \tag{B.3}$$

$$\frac{\partial^2 \bar{\varepsilon}_{ij}}{\partial x_1 \partial x_2} = \begin{pmatrix} \frac{\partial^2 \bar{\varepsilon}_{11}}{\partial x_1 \partial x_2} & \frac{\partial^2 \bar{\varepsilon}_{12}}{\partial x_1 \partial x_2} \\ \frac{\partial^2 \bar{\varepsilon}_{21}}{\partial x_1 \partial x_2} & \frac{\partial^2 \bar{\varepsilon}_{22}}{\partial x_1 \partial x_2} \end{pmatrix} \qquad \frac{\partial^2 \bar{\varepsilon}_{ij}}{\partial x_2 \partial x_1} = \begin{pmatrix} \frac{\partial^2 \bar{\varepsilon}_{11}}{\partial x_2 \partial x_1} & \frac{\partial^2 \bar{\varepsilon}_{12}}{\partial x_2 \partial x_1} \\ \frac{\partial^2 \bar{\varepsilon}_{21}}{\partial x_2 \partial x_1} & \frac{\partial^2 \bar{\varepsilon}_{22}}{\partial x_2 \partial x_1} \end{pmatrix} \tag{B.4}$$

1. Linear Field:

The linear form of Fig. B.1 is plane shear deformation, according to

$$\bar{\boldsymbol{u}}(\boldsymbol{x}) = \begin{pmatrix} \frac{1}{2}x_2 \\ 0 \end{pmatrix} \tag{B.5}$$

In this Figure, the position of the RVE in the macroscopic medium, is $\boldsymbol{x} = \boldsymbol{0}$. According to the above

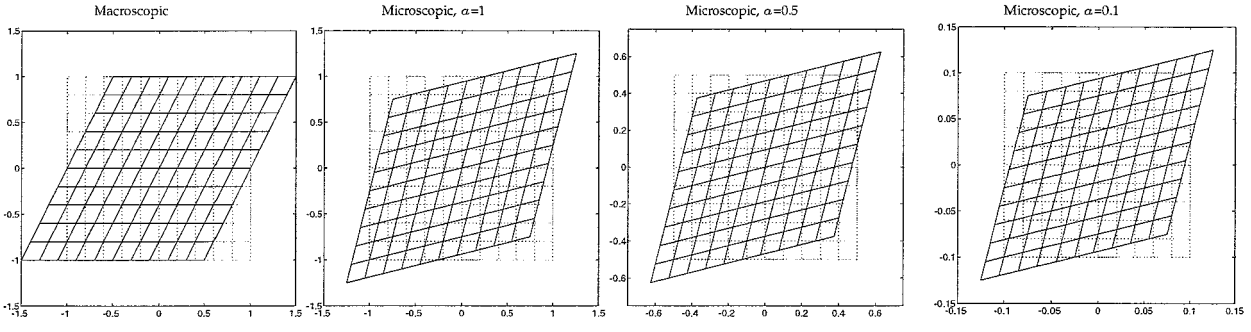

Figure B.1: Linear macroscopic displacement field

description:

$$\bar{\varepsilon}_{ij} = \begin{pmatrix} 0 & \frac{1}{4} \\ \frac{1}{4} & 0 \end{pmatrix} \qquad \frac{\partial \bar{\varepsilon}_{ij}}{\partial x_k} = 0 \qquad \frac{\partial^2 \bar{\varepsilon}_{ij}}{\partial x_k \partial x_l} = 0$$

$$\rightarrow \boldsymbol{u}(\boldsymbol{y}) = \begin{pmatrix} \frac{1}{4}y_2 \\ \frac{1}{4}y_1 \end{pmatrix}$$

Clearly, a macroscopic linear displacement field results in a microscopic linear displacement field, excluding influences of the chosen position of the RVE (because in the expression for $\boldsymbol{u}$, no macroscopic coordinates are present). Next, a cubic field will be applied on the macroscopic medium.

2. Cubic field:

A cubic displacement field can be formulated as follows:

$$\bar{\boldsymbol{u}}(\boldsymbol{x}) = \begin{pmatrix} \frac{1}{5}x_2^3 \\ \frac{1}{5}x_1^3 \end{pmatrix} \tag{B.6}$$

Following the same line as above:

$$\bar{\varepsilon}_{ij} = \begin{pmatrix} 0 & \frac{3}{10}(x_1^2 + x_2^2) \\ \frac{3}{10}(x_1^2 + x_2^2) & 0 \end{pmatrix}$$

$$\frac{\partial \bar{\varepsilon}_{12}}{\partial x_1} = \frac{3}{5}x_1 = \frac{\partial \bar{\varepsilon}_{21}}{\partial x_1} \qquad \frac{\partial \bar{\varepsilon}_{12}}{\partial x_2} = \frac{3}{5}x_2 = \frac{\partial \bar{\varepsilon}_{21}}{\partial x_2}$$

$$\frac{\partial^2 \bar{\varepsilon}_{12}}{\partial x_1^2} = \frac{3}{5} = \frac{\partial^2 \bar{\varepsilon}_{21}}{\partial x_1^2} \qquad \frac{\partial^2 \bar{\varepsilon}_{12}}{\partial x_2^2} = \frac{3}{5} = \frac{\partial^2 \bar{\varepsilon}_{21}}{\partial x_2^2}$$

$$\rightarrow \boldsymbol{u}(\boldsymbol{x}, \boldsymbol{y}) = \begin{pmatrix} \frac{3}{10}(x_1^2 + x_2^2 + x_1y_1 + x_2y_2)y_2 + \frac{1}{10}\left(y_1^2y_2 + y_2^3 - a^2(x_2 + 2y_2)\right) \\ \frac{3}{10}(x_1^2 + x_2^2 + x_1y_1 + x_2y_2)y_1 + \frac{1}{10}\left(y_1y_2^2 + y_1^3 - a^2(x_1 + 2y_1)\right) \end{pmatrix}$$

This expression is depicted in the Figs. B.2 and B.3. Fig. B.2 shows the dependency of the microscopic

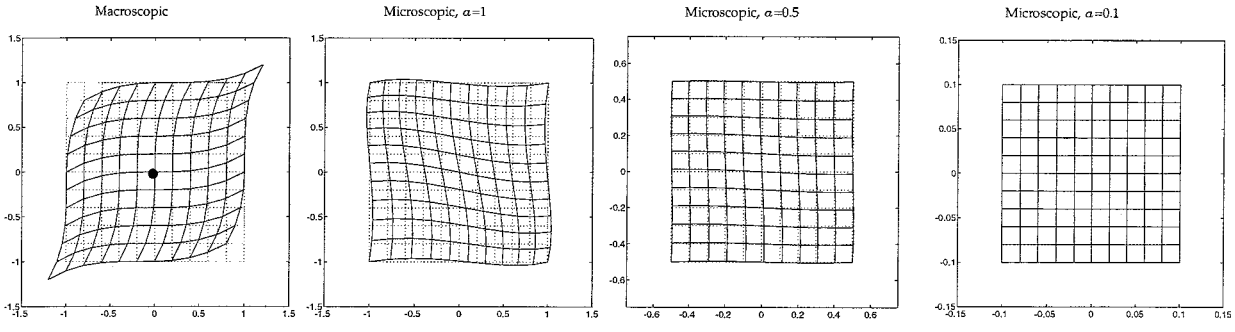

Figure B.2: Cubic displacement field, with RVE at $\boldsymbol{x} = \boldsymbol{0}$ (•)

scale parameter a. Hence, a decreasing RVE-size yields a gradually decreasing influence. This conclusion only is valid if the *products* $(a \times \partial \bar{\varepsilon}_{ij}/\partial x_k)$ and $(a^2 \times \partial^2 \bar{\varepsilon}_{ij}/\partial x_k \partial x_l)$ are small enough.

The macroscopic position dependency of the RVE on the microscopic displacements can be seen when comparing Fig. B.2 with Fig. B.3. Indeed, different microscopic fields follow from different positions in the continuum.

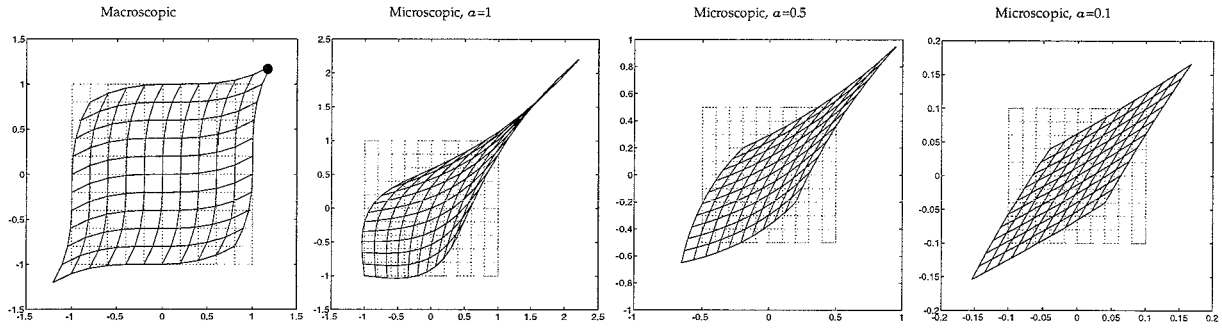

Figure B.3: Cubic displacement field, with RVE at $x = (a, a)$ (•)

Displacement field near a crack tip

In contrast to the preceding Section, we now turn our attention to a practical problem, viz. a crack tip. For this crack tip, an analytical displacement field is known and will be used here. This displacement field is derived under the assumption of linear elasticity. For further analytical treatment, we refer to Gdoutos (1993). We will look at both Mode I (i.e. tensile) as well as Mode II (i.e. shear) loadings.

Mode I loading

Here, we will turn our attention to the mode I loading case, i.e. a tensile test is executed on a specimen with an initial crack located at the edge. The analytical equations for that particular displacement field are given by:

$$\bar{u}_1(r,\theta) = \frac{K_I}{2\mu}\sqrt{\frac{r}{2\pi}}\cos\frac{\theta}{2}(\kappa - \cos\theta)$$
$$\bar{u}_2(r,\theta) = \frac{K_I}{2\mu}\sqrt{\frac{r}{2\pi}}\sin\frac{\theta}{2}(\kappa - \cos\theta)$$

In these equations, the appropriate fracture mechanics parameters are being used, i.e.:

- K: fracture toughness;
- r: distance from the crack tip;
- θ: angle with the horizontal;
- $\kappa = \begin{cases} 3 - 4\nu, & \text{for plane strain with } \nu \text{ Poisson's ratio;} \\ (3-\nu)/(1+\nu), & \text{for plane stress;} \end{cases}$
- $\mu = \dfrac{E}{2(1+\nu)}$ with E Young's modulus.

This displacement field is shown graphically in the left-hand picture of Fig. B.4. Typical microscopic responses can also be found in this Figure, with the location of the RVE in the macroscopic specimen represented by •. From this Figure, again, it can be seen that the microscopic fields are functions of the size of the RVE (a-size). In Fig. B.5, the RVE position is $(x_1, x_2) = (a/32, 0)$. Comparing this Figure with Fig. B.4, we can, again, conclude that a smaller RVE-size reduces the influence of the strain gradients. More meticulously, reducing the products ($a \times$*first strain derivative*) and ($a^2 \times$*second strain derivative*), results in a smaller impact of these terms on the deformation behaviour of the RVE. These analyses can also be performed for mode II loading.

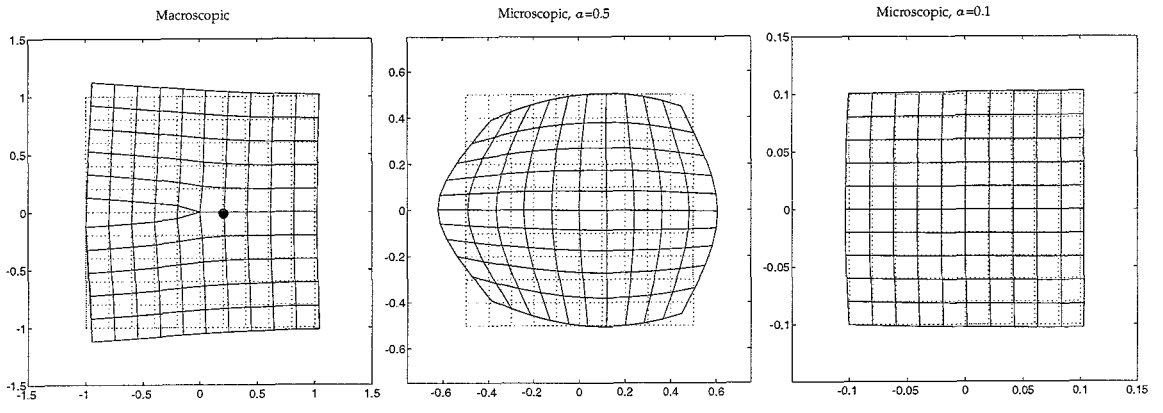

Figure B.4: Mode I loading, with the RVE at $\boldsymbol{x} = (a/5, 0)$ (•)

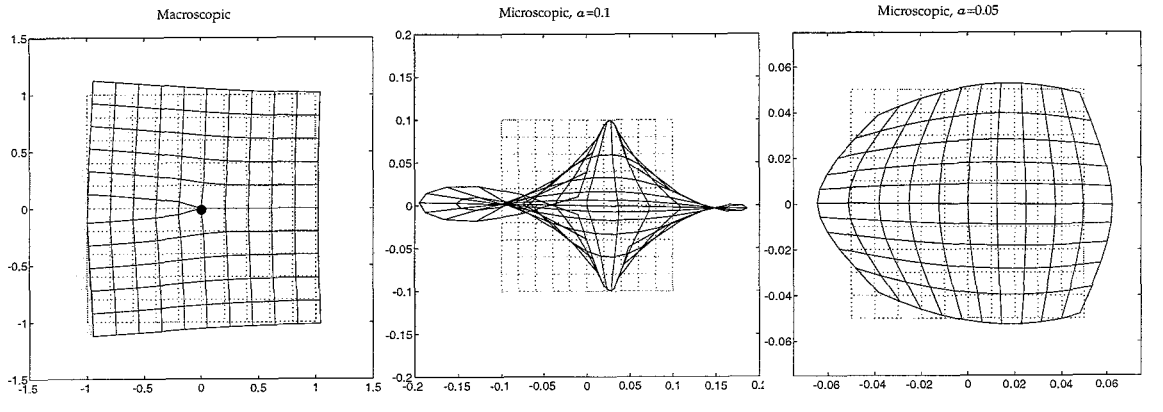

Figure B.5: Mode I loading, with the RVE at $\boldsymbol{x} = (a/32, 0)$ (•)

Mode II loading

The mode II loading case is a shear loading on a test specimen with an initial crack located at the edge, which can be observed in the left-hand picture of Fig. B.6. The equations for the displacement field are given by

$$\bar{u}_1(r,\theta) = \frac{K_{II}}{2\mu}\sqrt{\frac{r}{2\pi}}\sin\frac{\theta}{2}(2+\kappa+\cos\theta)$$
$$\bar{u}_2(r,\theta) = \frac{K_{II}}{2\mu}\sqrt{\frac{r}{2\pi}}\cos\frac{\theta}{2}(2-\kappa-\cos\theta)$$

In this loading case we too approach the cracktip by reducing r, resulting in larger strain gradients, as was the case in the mode I loading, see Fig. B.7.

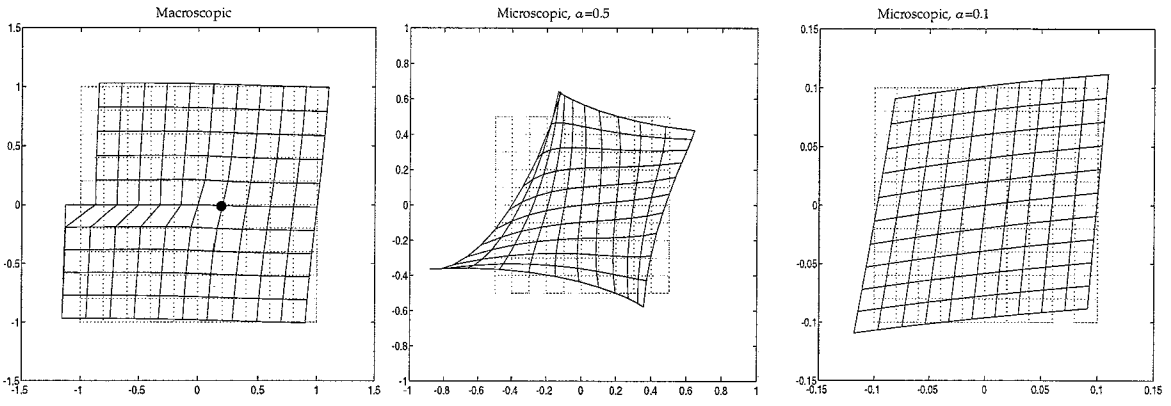

Figure B.6: Mode II loading, with the RVE at $\boldsymbol{x} = (a/5, 0)$ (•)

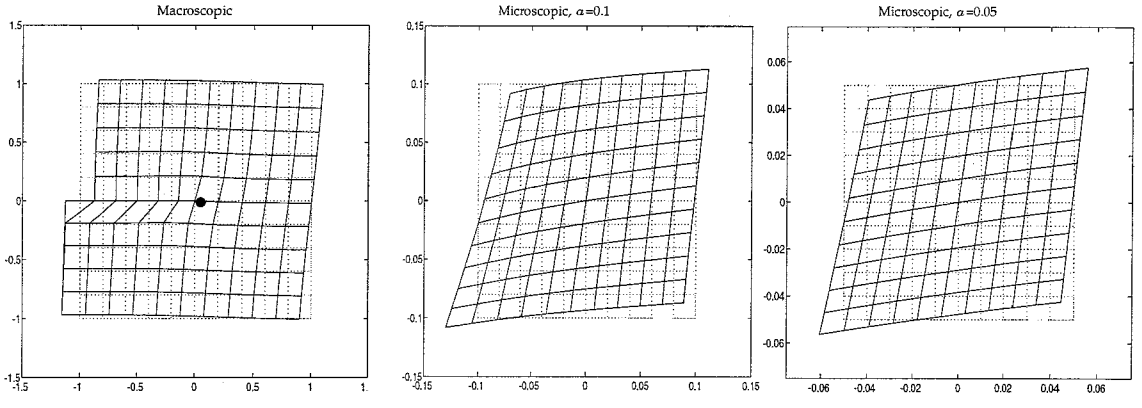

Figure B.7: Mode II loading, with the RVE at $\boldsymbol{x} = (a/8, 0)$ (•)

C The Global Strain-Displacement Matrix

The relation between the displacements and the strains can be put in matrix notation

$$\underset{\sim}{\varepsilon} = \underline{L}\,\underset{\sim}{u}. \tag{C.1}$$

Looking at equation (3.5), we can write the following

$$\begin{pmatrix} \varepsilon_{11} \\ \varepsilon_{22} \\ \varepsilon_{12} \\ \varepsilon_{21} \\ \kappa_{13} \\ \kappa_{23} \end{pmatrix} = \begin{pmatrix} \dfrac{\partial}{\partial x_1} & 0 & 0 \\ 0 & \dfrac{\partial}{\partial x_2} & 0 \\ 0 & \dfrac{\partial}{\partial x_1} & -1 \\ \dfrac{\partial}{\partial x_2} & 0 & 1 \\ 0 & 0 & \dfrac{\partial}{\partial x_1} \\ 0 & 0 & \dfrac{\partial}{\partial x_2} \end{pmatrix} \begin{pmatrix} u_1 \\ u_2 \\ \varphi \end{pmatrix}. \tag{C.2}$$

Using the discretizations of (3.36), we now obtain the following,

$$\underset{\sim}{\varepsilon}(\underset{\sim}{u}) = \underline{B}\,\underset{\sim}{u}^e \tag{C.3}$$

$$= \begin{pmatrix} \dfrac{\partial N_a}{\partial x_1} & 0 & 0 \\ 0 & \dfrac{\partial N_a}{\partial x_2} & 0 \\ 0 & \dfrac{\partial N_a}{\partial x_1} & -N_a \\ \dfrac{\partial N_a}{\partial x_2} & 0 & N_a \\ 0 & 0 & \dfrac{\partial N_a}{\partial x_1} \\ 0 & 0 & \dfrac{\partial N_a}{\partial x_2} \end{pmatrix} \underset{\sim}{u}^e. \tag{C.4}$$

With the aid of the Jacobian matrix, we can transform this matrix in terms of local quantities, that is, quantities in terms of ξ, η. The Jacobian matrix in interpolated notation is

$$\underline{J} = \begin{pmatrix} \displaystyle\sum_{a=1}^{n_{nd}} \left.\frac{\partial N_a}{\partial \xi}\right|_i x_a & \displaystyle\sum_{a=1}^{n_{nd}} \left.\frac{\partial N_a}{\partial \xi}\right|_i y_a \\ \displaystyle\sum_{a=1}^{n_{nd}} \left.\frac{\partial N_a}{\partial \eta}\right|_i x_a & \displaystyle\sum_{a=1}^{n_{nd}} \left.\frac{\partial N_a}{\partial \eta}\right|_i y_a \end{pmatrix}. \tag{C.5}$$

Here, the index a represents the nodenumber, the index i the integration point number of the element, and n_{nd} is the number of nodes of one element.

When we calculate the matrix

$$\underline{N}_{,\xi} = \begin{pmatrix} \left.\dfrac{\partial N_1}{\partial \xi}\right|_i & \left.\dfrac{\partial N_1}{\partial \eta}\right|_i \\ \vdots & \vdots \\ \left.\dfrac{\partial N_{n_{nd}}}{\partial \xi}\right|_i & \left.\dfrac{\partial N_{n_{nd}}}{\partial \eta}\right|_i \end{pmatrix}, \tag{C.6}$$

we are able to calculate the following matrix, with the aid of the inverse of the Jacobian matrix,

$$\underline{N}_{,\boldsymbol{x}} = \underline{J}^{-1}.\underline{N}^{T}_{,\boldsymbol{\xi}} = \begin{pmatrix} \left.\frac{\partial N_1}{\partial x_1}\right|_i & \left.\frac{\partial N_1}{\partial x_2}\right|_i \\ \vdots & \vdots \\ \left.\frac{\partial N_{n_{nd}}}{\partial x_1}\right|_i & \left.\frac{\partial N_{n_{nd}}}{\partial x_2}\right|_i \end{pmatrix}. \tag{C.7}$$

With these components, we can 'assemble' the $\underline{B}$ matrix,

$$\underline{B} = \begin{pmatrix} \left.\frac{\partial N_1}{\partial x_1}\right|_i & 0 & 0 & \dots & 0 \\ 0 & \left.\frac{\partial N_1}{\partial x_2}\right|_i & 0 & \dots & 0 \\ 0 & \left.\frac{\partial N_1}{\partial x_1}\right|_i & -N_1\big|_i & \dots & -N_4\big|_i \\ \left.\frac{\partial N_1}{\partial x_2}\right|_i & 0 & N_1\big|_i & \dots & N_4\big|_i \\ 0 & 0 & \left.\frac{\partial N_1}{\partial x_1}\right|_i & \dots & \left.\frac{\partial N_4}{\partial x_1}\right|_i \\ 0 & 0 & \left.\frac{\partial N_1}{\partial x_2}\right|_i & \dots & \left.\frac{\partial N_4}{\partial x_2}\right|_i \end{pmatrix}. \tag{C.8}$$

The Derivatives of the Shape Functions

The derivatives of the shape functions, necessary to calculate the $\underline{B}$-matrix, are given by

$$\begin{aligned} \frac{\partial N_1}{\partial \xi} &= \frac{1}{4}(\eta - 1), & \frac{\partial N_2}{\partial \xi} &= \frac{1}{4}(1 - \eta), & \frac{\partial N_3}{\partial \xi} &= \frac{1}{4}(1 + \eta), & \frac{\partial N_4}{\partial \xi} &= -\frac{1}{4}(1 + \eta), \\ \frac{\partial N_1}{\partial \eta} &= \frac{1}{4}(\xi - 1), & \frac{\partial N_2}{\partial \eta} &= -\frac{1}{4}(1 + \xi), & \frac{\partial N_3}{\partial \eta} &= \frac{1}{4}(1 + \xi), & \frac{\partial N_4}{\partial \eta} &= \frac{1}{4}(1 - \xi). \end{aligned}$$

The Derivatives of the Equivalent Strain

The derivatives of the equivalent strain, necessary to calculate the element stiffness matrix, are given by

$$\begin{aligned} \frac{\partial \varepsilon_{eq}}{\partial \varepsilon_{11}} &= \frac{2\varepsilon_{11} - \varepsilon_{22}}{\varepsilon_{eq}}, & \frac{\partial \varepsilon_{eq}}{\partial \varepsilon_{22}} &= \frac{2\varepsilon_{22} - \varepsilon_{11}}{\varepsilon_{eq}}, & \frac{\partial \varepsilon_{eq}}{\partial \varepsilon_{12}} &= \frac{3\varepsilon_{12} + \varepsilon_{21}}{4\varepsilon_{eq}}, \\ \frac{\partial \varepsilon_{eq}}{\partial \varepsilon_{21}} &= \frac{3\varepsilon_{12} + \varepsilon_{21}}{4\varepsilon_{eq}}, & \frac{\partial \varepsilon_{eq}}{\partial \kappa_{13}} &= \frac{3\ell^2\kappa_{13}}{2\varepsilon_{eq}}, & \frac{\partial \varepsilon_{eq}}{\partial \kappa_{23}} &= \frac{3\ell^2\kappa_{23}}{2\varepsilon_{eq}}. \end{aligned}$$